(2)

DROPLET SIZING RESEARCH

ANNUAL REPORT

SDL No. 84-2286-06

21 March 1984

Prepared For:

Air Force Office of Scientific Research
Building 410
Bolling Air Force Base
Washington, D.C. 20332

F49620-83-C-0060

SPECTRON DEVELOPMENT LABORATORIES INC.

Approved for public release;
distribution unlimited.

UNCLASSIFIED

SECURITY CLASSIFICATION OF THIS PAGE

REPORT DOCUMENTATION PAGE

1a. REPORT SECURITY CLASSIFICATION UNCLASSIFIED	1b. RESTRICTIVE MARKINGS
2a. SECURITY CLASSIFICATION AUTHORITY	3. DISTRIBUTION/AVAILABILITY OF REPORT Approved for Public Release; Distribution is Unlimited.
2b. DECLASSIFICATION/DOWNGRADING SCHEDULE	
4. PERFORMING ORGANIZATION REPORT NUMBER(S) 84-2286-06	5. MONITORING ORGANIZATION REPORT NUMBER(S) AFOSR-TR- 85-0207
6a. NAME OF PERFORMING ORGANIZATION Spectron Development Laboratories, Inc. 6b. OFFICE SYMBOL (If applicable)	7a. NAME OF MONITORING ORGANIZATION AFOSR/NA
6c. ADDRESS (City, State and ZIP Code) 3303 Harbor Blvd., Suite G3 Costa Mesa, California 92626	7b. ADDRESS (City, State and ZIP Code) Bolling AFB, DC. 20332
8a. NAME OF FUNDING/SPONSORING ORGANIZATION Air Force Office of Scientific Research 8b. OFFICE SYMBOL (If applicable) NA	9. PROCUREMENT INSTRUMENT IDENTIFICATION NUMBER F49620-83-C-0060
8c. ADDRESS (City, State and ZIP Code) Bldg. 410 Bolling Air Force Base, DC 20332	10. SOURCE OF FUNDING NOS. PROGRAM ELEMENT NO.: 61102F; PROJECT NO.: 2308; TASK NO.: A3; WORK UNIT NO.:
11. TITLE (Include Security Classification) DROPLET SIZING RESEARCH	
12. PERSONAL AUTHOR(S) CECIL F HESS	
13a. TYPE OF REPORT ANNUAL 13b. TIME COVERED FROM 1-15-83 TO 1-15-84	14. DATE OF REPORT (Yr., Mo., Day) 21 MARCH 1984 15. PAGE COUNT 71
16. SUPPLEMENTARY NOTATION	
17. COSATI CODES FIELD / GROUP / SUB. GR.	18. SUBJECT TERMS (Continue on reverse if necessary and identify by block number) nonintrusive, single particle counter, doppler, particle size velocity, mass flux

19. ABSTRACT (Continue on reverse if necessary and identify by block number)

The objective of this research program is to advance the understanding of droplet sizing technology in combustion environments using light scattering.

Two techniques which offer great potential in the measurement of sprays are studied. The first is referred to as "IMAX", and it consists of a nonintrusive pulse height analyzer. The second is referred to as "visibility/intensity (V/I)," and it performs a size measurement by examining the visibility and the pedestal intensity of a Doppler burst. The research conducted over this past year indicated that the IMAX technique provided a larger dynamic range and higher accuracy than V/I. It also showed that the two-color IMAX concept provided a higher S/N primarily because of the high efficiency in spectrally separating the two signals.

20. DISTRIBUTION/AVAILABILITY OF ABSTRACT UNCLASSIFIED/UNLIMITED ☒ SAME AS RPT. ☐ DTIC USERS ☐	21. ABSTRACT SECURITY CLASSIFICATION Unclassified
22a. NAME OF RESPONSIBLE INDIVIDUAL LEONARD H CAVENY	22b TELEPHONE NUMBER (Include Area Code) (202) 767-4937 22c. OFFICE SYMBOL AFOSR/NA

DD FORM 1473, 83 APR EDITION OF 1 JAN 73 IS OBSOLETE.

UNCLASSIFIED

SECURITY CLASSIFICATION OF THIS PAGE

Results obtained with these techniques for two kinds of sprays are discussed. Excellent resolution and self-consistency was experienced with IMAX when measuring the same spray using three different size ranges. Both techniques showed excellent reolution when measuring bimodal and trimodal sprays. A probe volume algorithm was developed and tested, and it appears to be very promising in the measurement of mass flux and local number density.

Accession For	
NTIS GRA&I	☒
DTIC TAB	☐
Unannounced	☐
Justification	
By	
Distribution/	
Availability Codes	
Dist	Avail and/or Special
A-1	

TABLE OF CONTENTS

LIST OF FIGURES

LIST OF TABLES

1.0 INTRODUCTION

This annual report for the contract No. F49620-83-C-0060 to perform droplet measurement research covers the period 15 January 1983 to 15 January 1984.

During this first year of the contract considerable progress was experienced as indicated in the Statement of Work (Section 2.0). Two techniques referred to as V/I and IMAX were studied and since the two are reasonably independent the technical sections are divided to clearly identify the progress, achievements and limitations associated with each technique.

2.0 STATEMENT OF WORK

The statement of work as shown in the original proposal and contract is included here for the three years of the contract. Next to each task there is an asterisk (*) or a triangle (Δ), the asterisk indicating completion of the task and the triangle indicating that some work was done during this year.

2.1 Year 1 - Droplet Measurement Research (Basic Research Element)

*Task 1.0 - Evaluation and assessment of previous results to provide a basis of departure for the present research.

*Task 2.0 - Plan the research to study two advanced droplet sizing concepts (V/I and IMAX) both analytically and experimentally.

*Task 3.0 - Theoretical definition of the two concepts based on fundamental scattering theories.

*Task 4.0 - Breadboard experimental setups to test and study both techniques.

*Task 5.0 - Experimentally determine the intensity of the light scattered by droplets immersed in a Gaussian beam. Compare these results with present scattering theories and correlations.

*Task 6.0 - Explore signal characteristics of the two techniques under ideal conditions, and establish optimum regions of validity.

ΔTask 7.0 - Analyze above data and compare to the theoretical description obtained in Task 3.0, to determine optimum selection of parameters.

*Task 8.0 - Report the results of each of the program tasks and develop a publication for submittal to a referee journal.

2.2 Year 2 - Droplet Measurement Research (Basic Research Element)

Task 1.0 - Evaluate and assess previous year's results and recent relevant developments and re-establish the direction of the proposed investigation.

Task 2.0 - Plan the research for the second year based on information obtained to this point.

ΔTask 3.0 - Formulate an analytical model to compute the optical probe volume and check experimentally verify the result.

*Task 4.0 - Explore the signal characteristics of a monodispersed spray when laser beams are interfered by a real spray.

Task 5.0 - Evaluate how regions of established validity under ideal conditions are affected by beam blockage.

Task 6.0 - Formulate statistical analysis to predict the effect of spray blockage on signal characteristics.

*Task 7.0 - Define and establish a processing method for the concepts studied. Perform preliminary spray measurements.

Task 8.0 - Analyze above data and compare to the statistical model obtained in Task 6.0 to reassess the validity of the optimum parameters obtained under ideal conditions.

ΔTask 9.0 - Report the results of each of the program tasks and develop a publication for submittal to a referee journal.

2.3 Year 3 - Droplet Measurement Research (Basic Research Element)

Task 1.0 - Evaluate and assess developments and the results of the first two years and redefine the critical aspects of the research.

Task 2.0 - Plan the research for the third year based on available information. Consider alternative methods or new concepts.

ΔTask 3.0 - Perform measurements in real sprays and explore the signal characteristics and establish the limitations of the techniques.

ΔTask 4.0 - Test processing methods chosen during second year, in the presence of real sprays, and develop corrections if necessary.

ΔTask 5.0 - Compare the results obtained with the various methods for the same spray under various spray conditions.

Task 6.0 - Analyze above data in conjunction with statistical models to establish the limitations of the techniques.

Task 7.0 - Report the results of the entire program and develop a publication for submittal to a referee journal.

3.0 ASSOCIATED RESEARCH

3.1 Research Associated with the Visibility/Intensity Technique

The interferometric technique to measure the size and velocity of particles flowing in a fluid has been in existence for approximately one decade. Farmer[1] introduced the concept of using visibility for particle sizing in the forward scattering direction. Since then, many researchers have contributed to the development of the technique. Robinson and Chu[2], for instance, rederived Farmer's results using a more rigorous approach, and the definition of visibility through the first order Bessel function was confirmed experimentally in forward scatter. However, contrary to what was through at the time, this visibility relationship could not be used at any angle other than the forward or zero degree. Adrian and Orloff[3] showed that it could not be used in the backscatter mode as predicted by Mie scattering theory. This finding was also confirmed by Roberds[4], who in addition showed that the configuration of the receiving optics would also affect the relationship between visibility and size.

The biggest known limitation of the visibility technique was its inability to measure particles in a dense field. The main reason being that the probe volume when observed in the forward direction is big and, therefore, the criterion of single particle measurement is not always met. In addition, the technique dictated that the largest measurable droplet was of the order of the fringe spacing. This imposes a limitation of about 200 μm to the largest measurable particle and also results

in a large probe volume, since a minimum number of fringes is needed (typically 8) to accurately process a Doppler signal.

Bachalo[5] formulated a mathematical model based on classical optics where the Mie scattering is approximated with refraction, diffraction and reflection. That model was used to predict the visibility of spherical particles in off-axis directions. Experimental results using monodispersed droplets confirmed the validity of the model under many conditions. Pendleton[6] later confirmed these results using a sophisticated numerical model that utilizes the full Mie equations. Recent work conducted under this contract at Spectron Development Laboratories shows that there are two major limitations on the existing models. First, all the theories developed thus far predict the Mie scattering from beams of uniform intensity. Second, the formation of the fringe pattern at the probe volume may be affected by secondary scattering of particles immersed in the laser beams before they cross. As a result of these limitations, the relationship between visibility and size is not straight forward and considerable errors can be made. A model proposed by M. L. Yeoman et al[7] pursues the solutions of the above problems. It consists of two concentric interferometric patterns of two colors such that the small one establishes a region of the big one where the hyperbolic variation of the visibility is negligible. Also digital analysis of the signals helps establish some that are in error. The results reported here show that using the intensity of the pedestal of the scattered light in addition to the visibility will eliminate many of these errors, significantly improving measurement accuracy.

3.2 Research Associated with the IMAX Technique

Several nonintrusive single particle counters using absolute scattered light have been proposed and they can be divided into two groups. In the first group[9-11] Gaussian laser beams are used and various mathematical inversion techniques have been proposed to extract the true size distribution from the signal amplitude distribution. Several assumptions are needed to perform such inversion, such as assuming the form of the size distribution[9] or a uniform average velocity for all the particles regardless of size[10]. A method to account for pinhole masking has also been described[11]. The second group of NSPC's uses a probe volume of known illumination to avoid the ambiguity of particle position. The technique described here falls in this group. Several approaches have been proposed[7,12,13,14] to accomplish this task. Apertures are used to cut off the edges of the Gaussian beam and thus image a probe volume of almost uniform illumination[12,13]. One of the apertures[12] had, in addition, two wedges that when properly oriented can be used to obtain the velocity vector in two components (magnitude and direction). Ring-shaped probe volumes have also been produced[14] by a TEM_{01} laser and a ring-shaped aperture. The measurement volume is defined by the intersection of apertures in front of two photomultipliers.

4.0 THE VISIBILITY/INTENSITY TECHNIQUE

In this section we describe some of the problems associated with the visibility technique, and how many of these problems can be corrected or avoided combining the visibility with the intensity of the scattered light.

4.1 Errors in the Visibility Measurements

The prediction of the droplet size based on the visibility of the light scattered by the droplet crossing an interferometric pattern of fringes is dependent on the pattern itself. For a perfect system the fringe visibility should be 100% and the light scattered should be primarily of one type. There are, however, many reasons in practical environments that contribute to alter the fringe pattern and, therefore, confuse the relationship between visibility and size. The result is that apparent sizes instead of true sizes are often measured. As an example, droplets interacting with the laser beams before they cross will randomly reduce (or even destroy) the fringe visibility. If a droplet is measured at such time, it will appear bigger than its true size. There are several factors that produce an error in the visibility measurement and they are listed below. They are divided into two groups: the ones that reduce the visibility and the ones that increase it.

A) Factors that Reduce the Visibility

1) Particles prior to crossover destroy fringe contrast. This is a function of the spray density.

2) Beam excursions due to turbulent hot media.

3) Hyperboloidal reduction of visibility.

4) Reflection/refraction can add destructively for large droplets immersed in a nonuniform (typically Gaussian) beam.

5) Multiple particles in probe volume.

6) Increase in signal background. Normally from many little drops present in the probe volume.

7) Loss of fringe contrast due to faulty components (beamsplitter, etc.)

B) Factors that Increase the Visibility

1) Out of focus drops "masked" by the pinhole.

2) Low level signals in the presence of a noisy background.

3) High time rise on leading edge of signal.

4.2 Description of the V/I Technique

This technique makes use not only of the visibility of the signal but also the peak intensity of the pedestal. Both parameters are available in the signal and their cross-correlation can be used to eliminate faulty signals produced in many practical environments. This technique will especially prevent small particles (high visibility) from appearing as large. Figure 4.1 shows a Doppler trace where both the visibility and the peak intensity of the pedestal are defined. There is a correlation between the size of the droplet and the amount of scattered light given by Mie theory. This correlation can be used to eliminate signals with an apparently different size. The proposed logic is as follows: droplets that produce a certain visibility must have a given size; hence, they must scatter light with a given intensity (characterized by

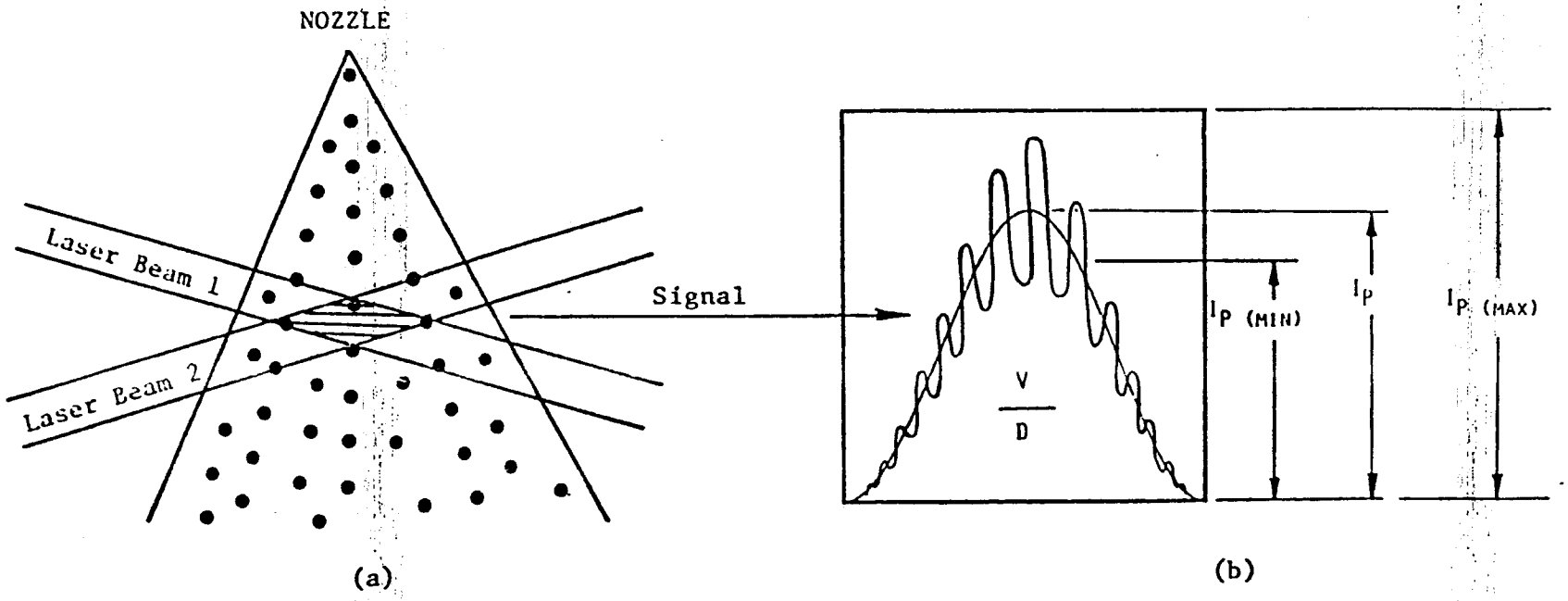

Figure 4.1. Schematic Representation of Doppler Burst Used in the Visibility/Intensity Technique.

I_p). Two exceptions are contemplated: first, droplets with the correct visibility will scatter different amounts of light due to the Gaussian nature of the probe volume's intensity; second, droplets with an erroneous visibility will not scatter light with an intensity corresponding to their apparent size.

The V/I method will then establish intensity limits for every measured visibility. This will produce a well established probe volume as a function of size and will reject droplets measured with an erroneous visibility. For instance, assume that the size corresponding to a visibility V_1 is d_1. Then the light scattered will have a pedestal with maximum intensity $I_{p_1}(max)$. Since this intensity would only be detected from droplets crossing through the middle of the probe volume, more relaxing limits are proposed. That is I_{p_1} will be accepted when $I_{p_1}(min)$ $I_{p_1}(min) < I_{p_1} < I_{p_1}(max)$. Obviously, the broader the limits, the larger the error that can be allowed with the visibility technique.

Figure 4.2 shows three cases that illustrate the correcting properties of the V/I method. Figure 4.2a shows a droplet of size d_1 with visibility V_1 and intensity I_{p_1}. Since this last one is within established limits, the signal is accepted as valid. Figure 4.2b shows the signal produced by a droplet of diameter d_2 but the visibility was reduced to V_1 due to fringe contrast reduction. Since the visibility is V_1, this signal would be interpreted as having a diameter d_1. However, the peak intensity of the pedestal I_{p_2} corresponds to its true size (d_2) and is smaller than $I_{p_1}(min)$ (to which it is compared) and hence, the signal is rejected. Figure 4.2c shows the signal of another droplet of

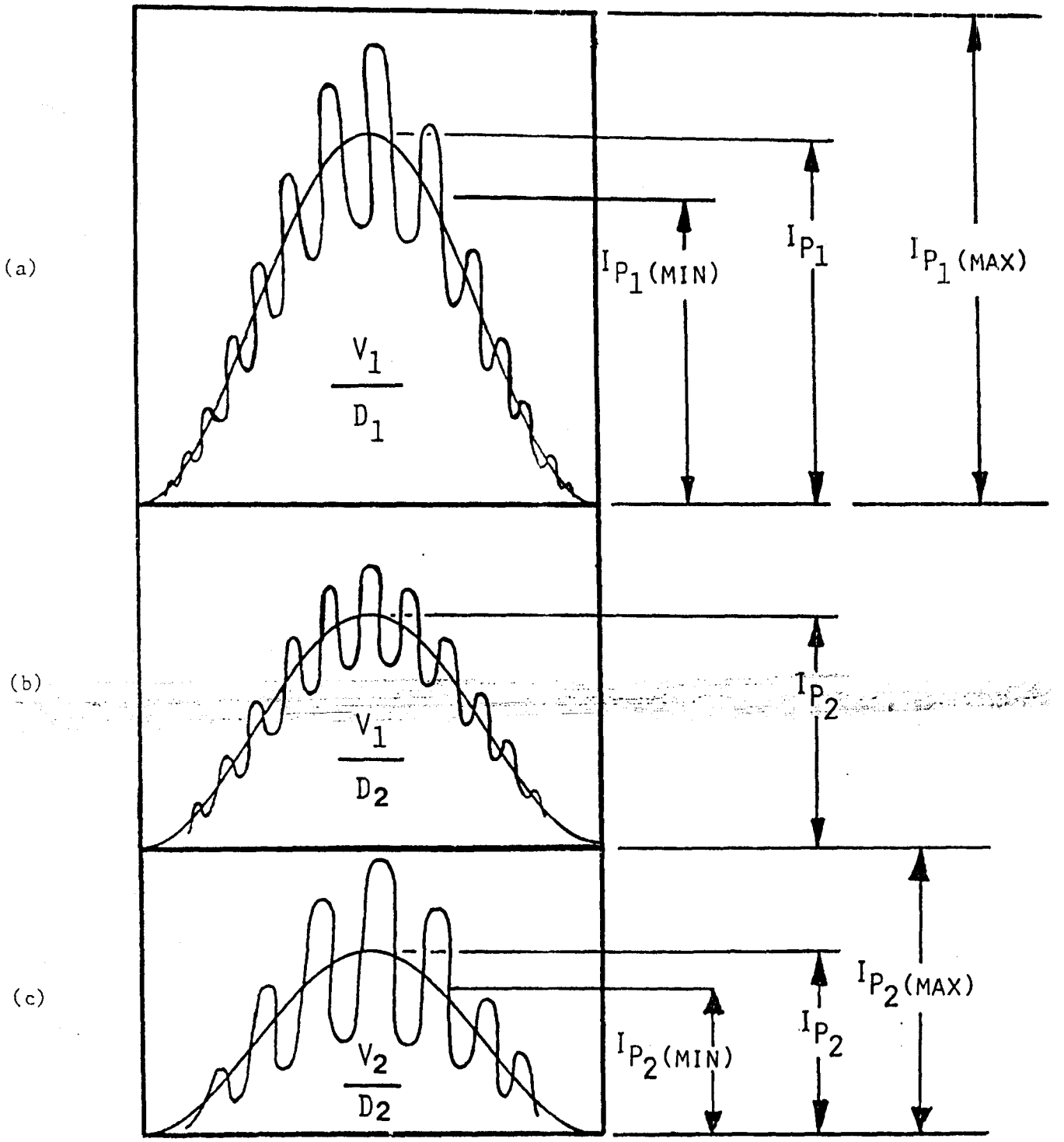

FIGURE 4.2. Visibility and Intensity of Two Size Droplets.

(a) and (c) correspond to droplets traveling thru the middle of an undisturbed probe volume; (b) could be from a small droplet traveling thru the middle of a disturbed probe volume or a large droplet traveling thru the edge of the Gaussian probe volume.

diameter d_2 but with correct visibility V_2 and corresponding pedestal I_{p_2}. This last one will also be accepted.

Since the intensity limits are functions of droplet size, a variable filter like the one shown on Figure 4.3 is necessary. It contains the intensity limits $I_p(\min)$, $I_p(\max)$ corresponding to any visibility V. Figures 4.4a and 4.4b show the raw data and software filtered data in an intensity/visibility plot. Figure 4.4a shows that the intensity is bounded by $I_p(\max)$ (with a few exceptions due to light re-radiated by upstream droplets). Points with different intensity/visibility combinations can be either due to droplets moving through the tail of the Gaussian intensity profile of the probe volume or to droplets with an erroneous visibility. By limiting the intensity of the pedestal for which a signal is considered valid, two things are accomplished: (1) the limits of the probe volume are carefully established; and, (2) most importantly, most of the signals with erroneous visibility are rejected.

4.3 Results Obtained with the V/I Technique

Experimental results are presented to illustrate the accuracy and resolution of the visibility/intensity technique, and how it compares with visibility only.

Effect of Beam Blockage on Size Distribution

The effect of a very dense spray blocking the laser beams before the probe volume was studied. Figure 4.5a shows the histogram produced

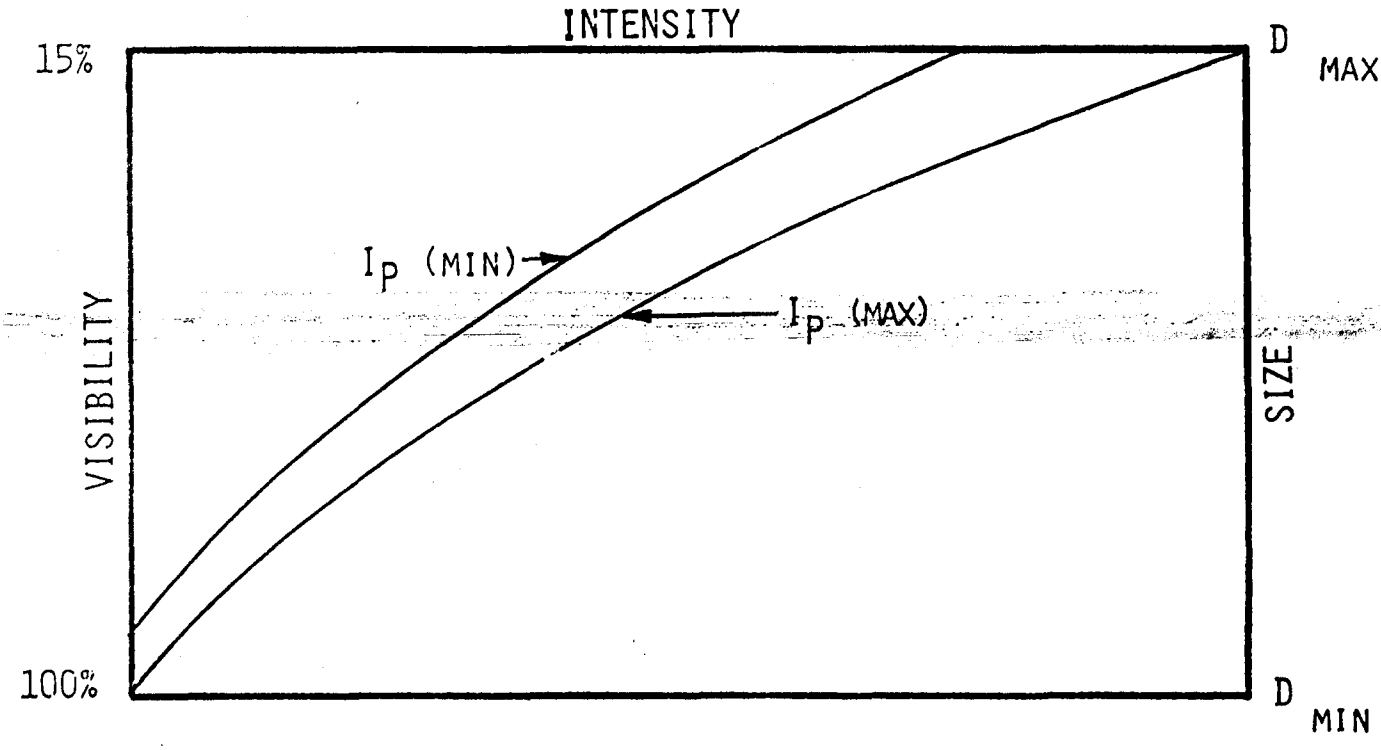

FIGURE 4.3. VARIABLE INTENSITY VS. VISIBILITY SOFTWARE FILTER

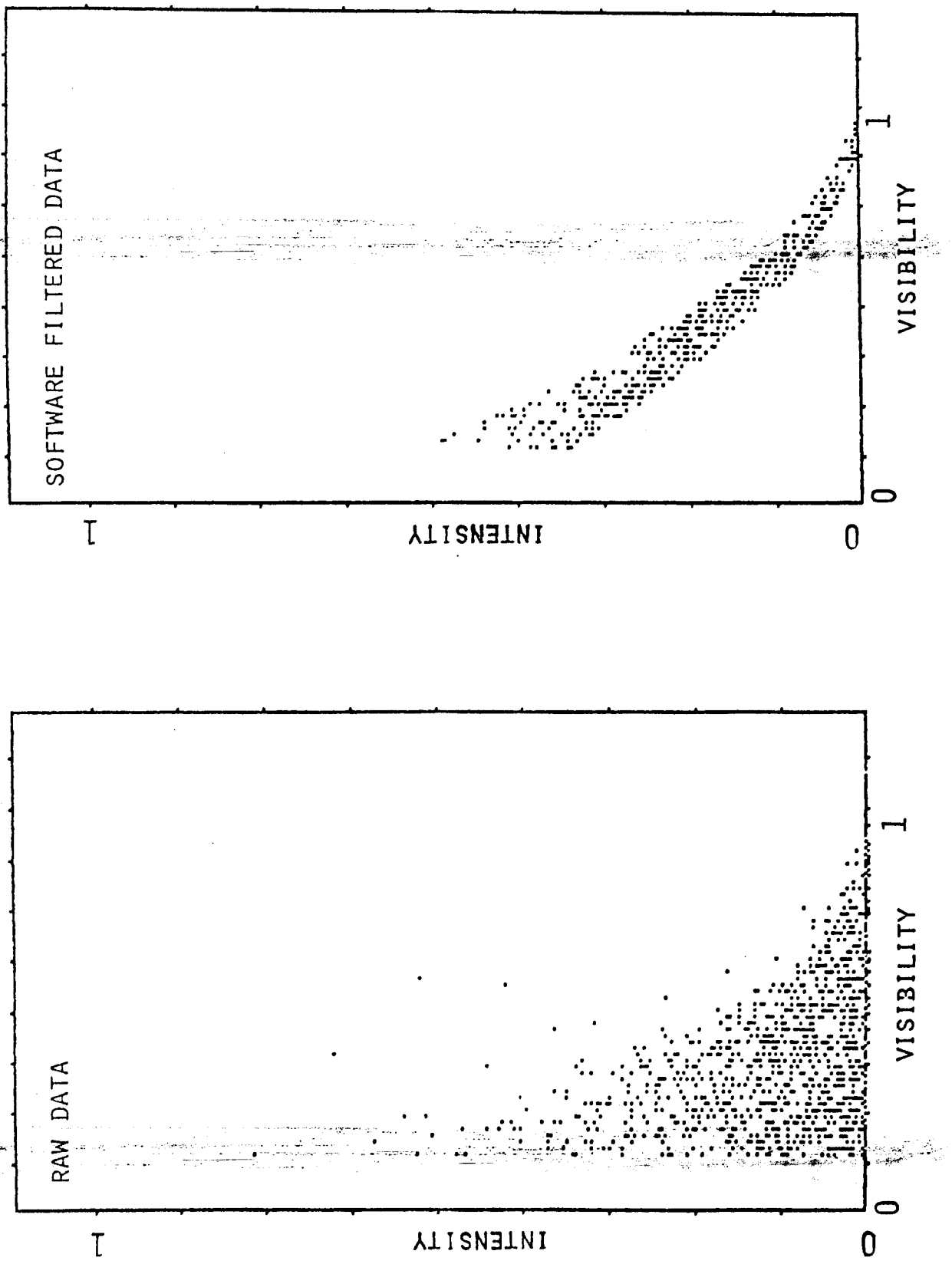

FIGURE 4.4. PRELIMINARY RESULTS OF VISIBILITY/INTENSITY ASSESSMENT

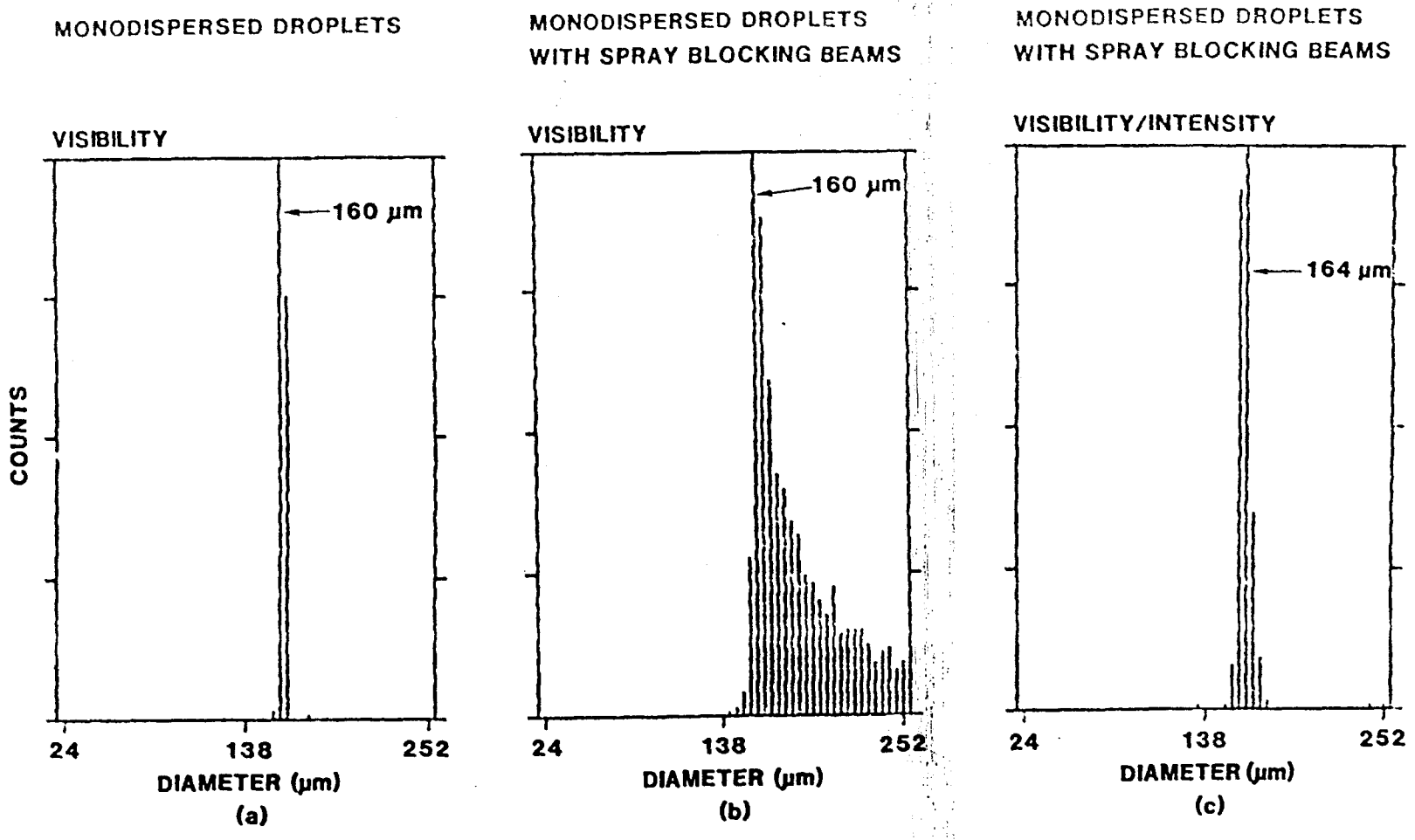

FRINGE SPACE= 37 μm
f No.= 5
θ=30°

FIGURE 4.5. SIZE DISTRIBUTIONS OF A MONODISPERSED STRING OF DROPLETS.
(a) Monodispersed Droplets Measured with V/I, No Spray Blockage
(b) Monodispersed Droplets Measured with Visibility Only. Blocking Spray Before Crossing.
(c) Monodispersed Droplets Measured with V/I. Blocking Spray Before Crossover.

when monodispersed droplets travel through the middle of an undisturbed probe volume. Figure 4.5b shows a histogram obtained with the visibility technique of the same monodispersed droplets but now the laser beams have traveled through a real spray before crossing. We made sure that the spray was not going into the probe volume. The fringe pattern produced by crossing two laser beams is well behaved and theoretically predicted in the undisturbed case. However, when the beams travel through a spray, this fringe pattern can be considerably altered due to random beam blockage. The result can be a distorted Doppler signal with a visibility, both lower and higher than that predicted theoretically. Considerable error in the size distribution will then be observed. The size of the error depends on the visibility itself. It is quite apparent from the histograms that what should be a monodispersed distribution is measured as a very broad one. The next histogram shown on Figure 4.5c shows the results obtained with V/I when the beams travel through the spray before crossing (same conditions as Figure 4.5b). Notice that a very narrow distribution is thus obtained.

V/I Measurements with the Berglund-Liu Droplet Generator

The calibration and verification source used in these experiments was the Berglund Liu monodisperse droplet generator. This generator can work in two modes: (a) it can generate a string of droplets of known size and equally spaced at the measurement point; (b) using a cap and dispersion air, these droplets can be dispersed into a spray of monodispersed droplets.

It has been observed in previous studies[8] that under some dispersion air conditions, some of the droplets will collide and form other droplets with double or even triple the volume. Therefore, if the primary droplet diameter is d_o, then droplets with diameter $2^{1/3}d_o$ and $3^{1/3}d_o$ can be produced. It must be pointed out that in these studies, we did not obtain photographic measurements to verify the presence of the secondary droplets. The size of the primary droplets was accurately predicted from the flow rate and frequency of vibration of the pinhole.

One limitation imposed by the Berglund Liu is that it cannot produce droplets of a given size at arbitrary spacing. Since the measurement instrument requires the presence of only one droplet in the probe volume, that limits the size droplet that can be measured.

The procedure used in these experiments was to produce a string of large monodispersed droplets to calibrate the instrument. Then smaller droplets were produced by increasing the frequency of vibration of the orifice, and with the dispersion air a spray of these droplets was formed. Typical number density at the probe volume was 500 droplets/cc, and the diameter of the spray at the plane of measurements was about 4 mm.

A DSI system with V/I capability was used to obtain the data shown below.

Optical configuration:

- Collection angle of 30°
- Transmitting lens = 495 mm
- Waist diameter = 300 μm
- Fringe spacing = 13.6 μm
- Collection F# = 5

The high voltage to the photomultiplier was established with a droplet string of diameter 100 μm.

The size range of interest was 9 to 92 μm.

A spray of droplets with primary diameter of 53 μm was then produced using the Berglund Liu with a flow rate of 0.21 cc/min and frequency of 45.8K Hz and the dispersion air. For the conditions selected above, this size will produce a visibility of 58%.

Notice that for primary droplets of 53 μm, the droplets will have a diameter of $2^{1/3}$ x 53 = 66 μm, and the triplets' diameter will be $3^{1/3}$ x 53 = 76 μm.

Results are shown for both visibility/intensity and visibility only to provide some comparison.

Figure 4.6 shows the measurements of the monodispersed spray of 53 μm.

Figure 4.7a shows the data of the spray formed of primary droplets and doublets.

Figure 4.7b shows results similar to Figure 4.7a but obtained with visibility only. Notice how much broader the distributions are.

Figure 4.7c shows a spray containing primary droplets, doublets and triplets.

Figure 4.7d shows results similar to Figure 4.7c but obtained with visibility only. Notice that the distribution is broader and the resolution is not as fine.

Both the accuracy and resolution of these measurements are very good. The theoretically predicted sizes are 53 μm , 66 μm, and 76 μm. The corresponding measured diameters are (52 to 54), (63 to 65), and 73 μm.

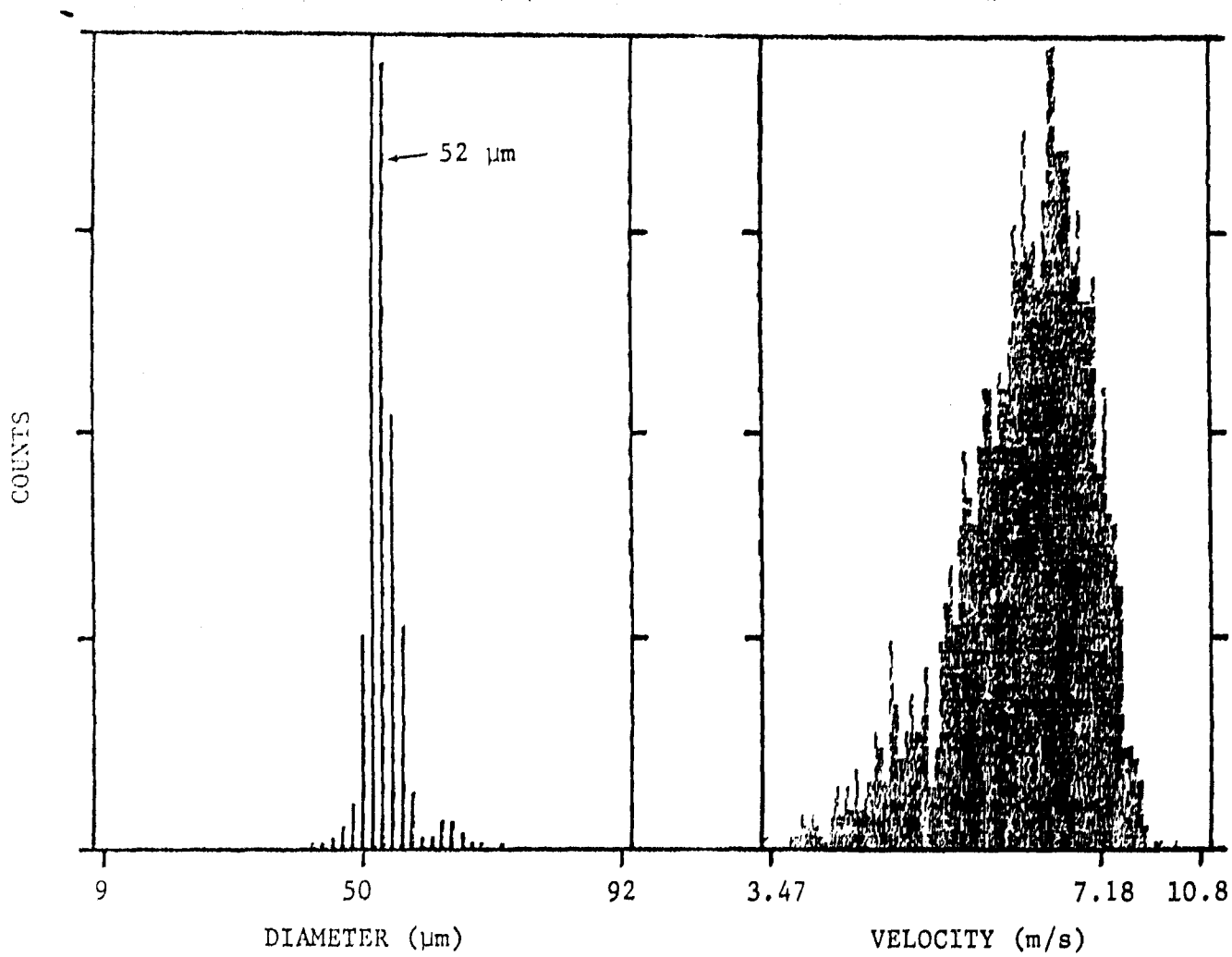

FIGURE 4.6. VISIBILITY/INTENSITY MEASUREMENTS OF MONODISPERSED SPRAY

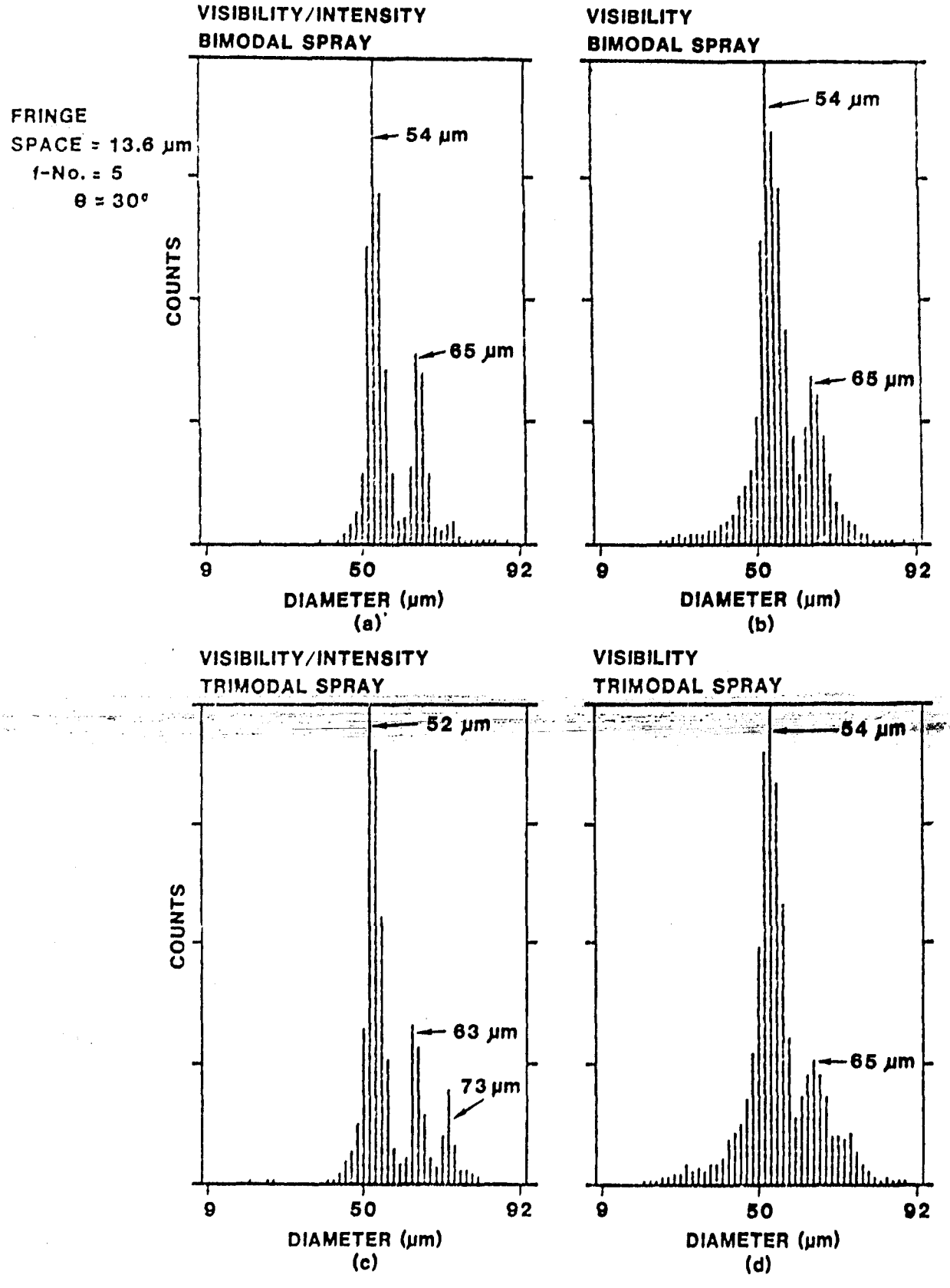

FIGURE 4.7. SIZE DISTRIBUTIONS OF BIMODAL AND TRIMODAL SPRAYS WITH VISIBILITY AND VISIBILITY/INTENSITY

4.4 The V/I Probe Volume

An important aspect of any optical technique is the recognition and determination of the probe volume. The implication is that different size particles scatter different amounts of light (typically proportional to the square of the diameter). Also, the intensity of the probe volume is non-uniform (typically Gaussian). Therefore, for a given threshold level the volume of detectability is a function of particle size. This will introduce a natural bias in the histogram of particle size. To correct this bias the probe volume needs to be computed as a function of particle size and optical configuration and then used to correct the biased histogram.

A	:	area of measuring region
b_o	:	waist radius
CF	:	collection factor
D_p	:	diameter of pinhole
D_{laser}	:	diameter of laser
d	:	diameter of droplet
d_o	:	maximum droplet diameter ($d_o/\delta CF$) = .845) for a given size range
f	:	focal length of transmitting lens
f_1	:	focal length of 1st collecting lens
f_2	:	focal length of 2nd collecting lens
I_{Th}	:	ground to peak threshold (front panel in volts)
I_s	:	d_c saturation (0.65 volts)
N	:	fringes required by processor (front panel)
P	:	pedestal intensity
V	:	visibility of size d
V_o	:	visibility of size d_o (V_o = .151)
x	:	coordinate normal to fringes

y,z : coordinates

δ : fringe spacing

γ : crossover angle

θ : angle of collection

4.5 Simplified Probe Volume Model

The cross-sectional area is given by:

$$A = \frac{2D_p y}{\sin\theta} \cdot \frac{f_1}{f_2} \qquad (1)$$

where y must be calculated based on the Gaussian profile and d (droplet diameter).

Let us call I_s the saturation level imposed by the electronics. Then for the largest detectable droplet:

$I_{peak} \leq I_s$.

The intensity profile of a probe volume formed by crossing two Gaussian beams is given by:

$$I = 2I_o \exp\left\{ \left(\frac{-2}{b_o^2}\right) \left[x^2+y^2 + \frac{z^2\gamma^2}{4}\right] \right\} \cdot$$

$$\left[\cos h \left(\frac{2 \times z\gamma}{b_o^2}\right) + \cos \frac{4\pi \times \sin\left(\frac{\gamma}{2}\right)}{\lambda} \right] \cdot$$

For a pinhole limited signal, we can assume z to be small; therefore,

$$I \approx 2I_o \exp\left[\left(\frac{-2}{b_o^2}\right)(x^2+u^2)\right] \cdot \left[1 + \cos\frac{z\pi\gamma x}{\lambda}\right] \quad .$$

The pedestal scattered by the droplet of diameter d is given by:

$$P = 2I_o K_o d^2 \exp\left[\left(\frac{-2}{b_o^2}\right)(x^2+y^2)\right] \quad .$$

The intensity scattered by the same droplet is given by:

$$I_s = 2I_o K_o d^2 \exp\left[\left(\frac{-2}{b_o^2}\right)(x^2+y^2)\right]\left[1 + \frac{\cos 2\pi\gamma x}{\lambda} \cdot V\right] \qquad (2)$$

The peak intensity occurs at x=0, y=0; and for the largest droplet,it is given by:

$$Ipeak = 2I_o K_o d_o^2(1 + V_o) < I_s \quad .$$

Solving for I_o:

$$I_o = \frac{I_s}{2K_o d_o^2 (1 + V_o)} \quad . \qquad (3)$$

The expression for the peak-to-peak intensity I_{ac} can be obtained by setting the cosine term to +1 and -1 in Equation 2, and then subtracting:

$$\therefore \quad I_{ac} = 4I_o K_o V d^2 \exp \left[\left(\frac{-2}{b_o^2}\right) (x^2 + y^2) \right] \quad .$$

Substituting Equation 3 in the above equation, we get:

$$I_{ac} = \frac{2d^2 V I_s}{d_o^2 (1+V_o)} \exp \left[\left(\frac{-2}{b_o^2}\right) (x^2 + y^2) \right] \qquad (4)$$

and

$$P = \frac{d^2 I_s}{d_o^2 (1 + V_o)} \exp \left(\left[\frac{-2}{b_o^2}\right) (x^2 + y^2) \right] \quad . \qquad (5)$$

In the old probe volume model, it was sufficient that $I_{ac} > I_{min}$. The new intensity/visibility software filter, however, limits the intensity further by limiting the pedestal of acceptability.

To criterion that $I_{ac} > I_{min}$ is absolutely necessary but not sufficient, except for the first 4 bins which have no minimum pedestal intensity limitation.

The intensity/visibility software filter, which is contained in Table 1, was constructed such that P_{max} is proportional to d_{max}^2. For instance for bin 35, $d_{max} = .595$ and $P_{max} = 271$. For bin 8, $d_{max} = .2185$.

$$\therefore \quad P_{max_8} = \left(\frac{.2185}{.595}\right)^2 \times 271 = 36.5$$

Given that the visibility falls in any one bin, the actual pedestal scattered by the droplet has to fall between P_{min} and P_{max}, where P_{max} corresponds to the droplet moving through the center $x = y = z = 0$ of the probe volume. Given this visibility V there is a bin # associated which corresponds to a diameter d (as given by the visibility Table 2). The intensity/visibility software filter (included in Table 1) imposes the condition:

$$P = \frac{d^2 I_{s_1}}{d_o^2 \left(1+V_o\right)} \exp\left(\frac{-2y^2}{b_o^2}\right) > P_{min}$$

TABLE 1. VISIBILITY INTENSITY TABLE

BIN NO.	I_{MIN} (mV)	I_{MAX} (mV)	BIN NO.	I_{MIN} (mV)	I_{MAX} (mV)
1	0	16	40	225	348
2	0	17	41	235	362
3	0	20	42	247	378
4	0	23	43	258	394
5	4	25	44	269	410
6	6	27	45	280	427
7	9	33	46	293	443
8	11	37	47	305	460
9	14	42	48	317	479
10	18	46	49	329	495
11	21	51	50	343	515
12	25	57	51	355	533
13	28	63	52	368	550
14	33	69	53	382	571
15	37	75			
16	42	82			
17	47	90			
18	52	97			
19	57	105			
20	63	114			
21	69	122			
22	75	131			
23	81	139			
24	87	149			
25	95	160			
26	101	170			
27	108	180			
28	116	191			
29	124	203			
30	132	214			
31	140	225			
32	149	237			
33	158	251			
34	167	264			
35	175	277			
36	184	290			
37	194	304			
38	205	318			
39	215	332			

TABLE 2. THE VISIBILITY FUNCTION

BIN NO.	VIS LOW	VIS HI	REL BW	DIA/ DELTA*CF
1	.986	.989	4	.0813
2	.981	.985	5	.096
3	.975	.98	6	.1107
4	.968	.974	7	.1254
5	.961	.967	7	.1401
6	.953	.96	8	.1548
7	.944	.952	9	.1695
8	.935	.943	9	.1842
9	.924	.934	11	.1989
10	.914	.923	10	.2136
11	.902	.913	12	.2283
12	.89	.901	12	.243
13	.877	.889	13	.2577
14	.864	.876	13	.2724
15	.85	.863	14	.2871
16	.835	.849	15	.3018
17	.82	.834	15	.3165
18	.804	.819	16	.3312
19	.788	.803	16	.3459
20	.772	.787	16	.3606
21	.755	.771	17	.3753
22	.737	.754	18	.39
23	.72	.736	17	.4047
24	.701	.719	19	.4194
25	.683	.7	18	.4341
26	.664	.682	19	.4488
27	.645	.663	19	.4635
28	.626	.644	19	.4782
29	.606	.625	20	.4929
30	.587	.605	19	.5076
31	.567	.586	20	.5223
32	.547	.566	20	.537
33	.527	.546	20	.5516
34	.506	.526	21	.5664
35	.486	.505	20	.5811
36	.466	.485	20	.5958
37	.446	.465	20	.6104
38	.425	.445	21	.6252
39	.405	.424	20	.6399
40	.385	.404	20	.6546
41	.365	.384	20	.6692
42	.345	.364	20	.684
43	.326	.344	19	.6987
44	.306	.325	20	.7134
45	.287	.305	19	.728
46	.268	.286	19	.7428
47	.249	.267	19	.7575
48	.231	.248	18	.7722
49	.213	.23	18	.7868
50	.195	.212	18	.8016
51	.177	.194	18	.8163
52	.16	.176	17	.831
53	.143	.159	17	.8456

where P is measured by a peak detector of the Gaussian envelope and, therefore, it corresponds to x=0. I_{s_1} and P_{max} correspond to each other.

d_{min}	d_{max}
$P_{min} = 0.7\ P(d_{min})/_{max}$	P_{max}

Given a bin #, there is a correspondence between diameter and pedestal,

where: $$P(d_{min})/_{max} = \frac{d_{min}^{2} I_{s_1}}{d_o^{2}(1+V_o)} e^{0} \quad ,$$

$$\therefore \quad P_{min} = \frac{0.7\ d_{min}^{2} I_{s_1}}{d_o^{2}\ (1+V_o)} \quad .$$

Therefore, $$I_{s_1} = \frac{d_o^{2}(1+V_o) P_{min}}{0.7\ d_{min}^{2}} = \frac{d_o^{2}(1+V_o)\ P_{max}}{d_{max}^{2}} \quad .$$

Substituting for I_{s_1} above:

$$P = \frac{d^{2}\ P_{max}}{d_{max}^{2}} \exp\left(\frac{-2y^{2}}{b_o^{2}}\right) > P_{min} \quad .$$

Solving for y

$$y = \sqrt{-\frac{b_o^2}{2} \ln \left(\frac{P_{min}}{Kd'^2}\right)} \quad , \qquad (6)$$

where $K = \left.\frac{P_{max}}{d'^2_{max}}\right|$ at any bin # .

For instance for bin #35, $K = \frac{.271}{.595^2} = .765$.

Note that the value of y will only remain constant if the characteristic size is d'_{min}, in which case

$$\frac{P_{min}}{d'^2_{min}} = 0.7\ K \quad ,$$

and $$y = \sqrt{-\frac{b_o^2}{2} \ln 0.7} = .42\ b_o \quad .$$

However, I have chosen $d_{charact}$ to be the value given in the visibility table, which is larger than d_{min}; therefore $y > 0.42$. For the high visibility bins, $d_{charact} >> d_{min}$; and, therefore, we should expect $y >> .42$ as shown in the example. The expression for y based on the threshold and saturation intensity is given by:

$$y < \sqrt{-\frac{b_o^2}{2} \ln \left[\frac{I_{Th}}{I_s} \left(\frac{d_o}{d}\right)^2 \frac{(1+V_o)}{V}\right] - x^2} \qquad (7)$$

Example

For the conditions:

$I_{Th} = .0005V$

$I_s = .63V$

$d_o' = .845$

$V_o = .151$

$x \approx b_o$

Also from Table 1 at bin # 35, d' = .595 and $P_{max} = .271V$ at y = 0.

$$I_{s_1} = \frac{P\, d_o^2 (1+V_o)}{d^2} = \frac{.271(.845)^2 (1.151)}{.595^2} = .63V \quad .$$

$$K = \frac{.271}{.595^2} = .765 \quad .$$

Therefore, Equation 6 yields: $$y = \sqrt{-\frac{b_o^2}{2} \ln \left(\frac{P_{min}}{.765 d'^2}\right)}$$

where P_{min} is given in volts.

Equation 7 yields:

$$y \leq b_o \sqrt{-\frac{1}{2} \ell n \left[\frac{6.3 \times 10^{-4}}{d'^2 V}\right] - 1} \quad .$$

For example:

bin #	d'	v	P_{min}	$\frac{y(6)}{b_o}$	$y(7)/b_o$
53	.8456	.15	.373	.436	1.25
35	.5811	.49	.171	.44	1.34
13	.2577	.88	.0278	.55	1.12
5	.1405	.965	.0042	.8	.84
4	.1254	.97	0	0	.77

Notice that the relationship between y and bin # would be a constant if for P_{min} I used the corresponding d_{min} instead of the d given on the V Table.

5.0 THE IMAX TECHNIQUE

The method discussed here bases the size measurement on the absolute intensity scattered by the droplet crossing the probe volume, and the velocity measurement on the classical Doppler signal. It is referred to as the IMAX method. In situ single particle counters are limited because of the nonuniform profile (typically Gaussian) of laser beams. Under this condition a particle crossing the middle of the beam will scatter more light than a similar particle crossing through the edge. Therefore, the relationship between size and scattered light is not unique.

To circumvent this problem, two beams of unequal size are crossed such that the small beam identifies the middle of the large beam and therefore, removing the Gaussian ambiguity. Laser beams are chosen because of their spatial and temporal coherence and because of their size. These beams will interfere where they cross and a fringe pattern will be formed in the middle of the large beam. Signals exhibiting an ac modulation will have crossed the fringe pattern and therefore, the middle of the large beam. Both size and velocity of individual spherical particles can be extracted from this signal.

At least two approaches can be used to implement the above concept. The first consists of crossing two laser beams of different diameters but with the same wavelength. In the second two small beams of one wavelength cross in the middle of a larger beam of another wavelength. These approaches will now be explained starting with the second.

5.1 Two-Color System

Figure 5.1 illustrates the probe volume of this method. A spherical particle crossing through the fringes will also cross through a region of almost uniform intensity of the large beam. The ratio of the two beam diameters will establish the uniformity of the intensity incident on the droplet.

If we refer to the small beam as 1 and the large beam as 2, the intensity profiles in the probe volume can be spectrally separated, and given by:

$$I_1 = 2I_{o_1} \exp\left\{\left(\frac{-2}{b_{o_1}^2}\right)\left[x^2+y^2+z^2\gamma^2/4\right]\right\} \cdot \left[\cosh\left(\frac{2xy\gamma}{b_{o_1}^2}\right) + \cos\frac{4\pi x \sin\left(\frac{\gamma}{2}\right)}{\lambda}\right], \quad (8)$$

and

$$I_2 = I_{o_2} \exp\left[-\frac{2}{b_{o_2}^2}(x^2+y^2)\right] \quad . \quad (9)$$

Where I_o is the center intensity, γ is the intersection angle, b_o the waist radius, λ the laser wavelength, and x,y,z the coordinates. The z dependence of the large beam is neglibible. If we also assume that $\frac{z\gamma}{2} \approx 0$(which is an excellent assumption since a pinhole in the receiver

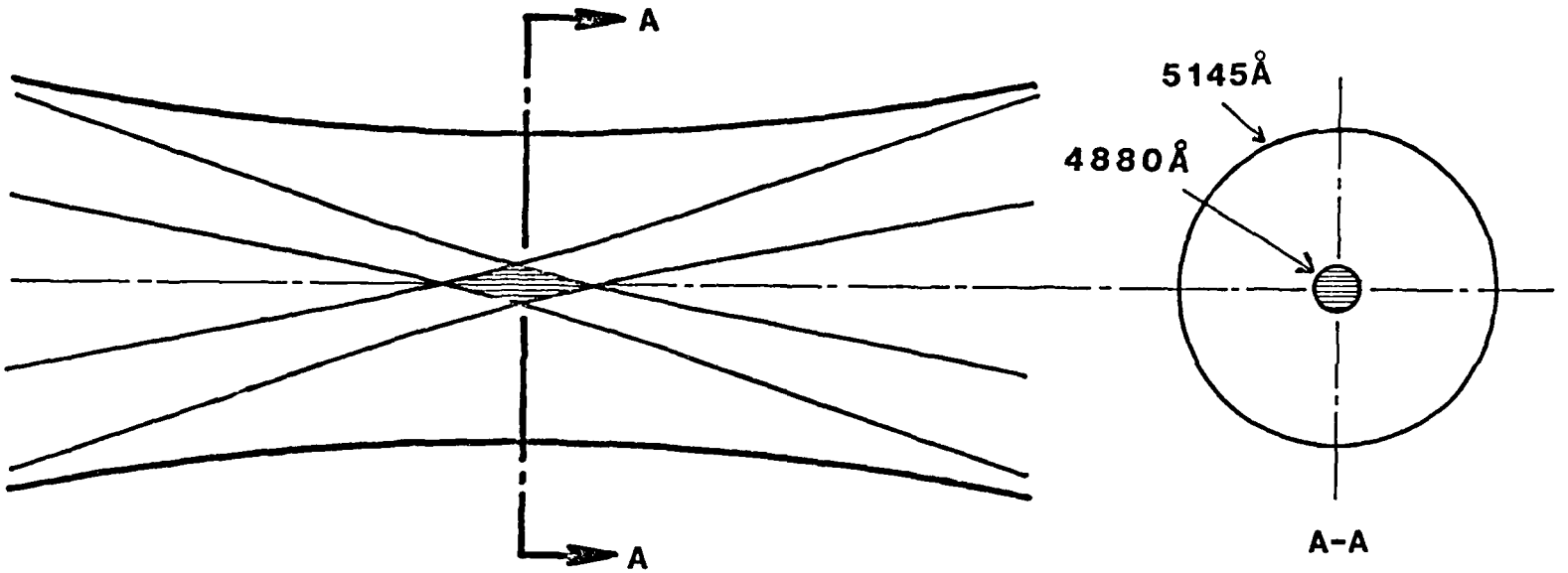

FIGURE 5.1. PROBE VOLUME OF TWO COLOR IMAX TECHNIQUE

will limit the value of z), the intensity scattered by a spherical particle is given by:

$$I_{s_1} = 2I_{o_1} K_{o_1} d^2 \exp\left[\left(-\frac{2}{b_{o_1}^2}\right)(x^2+y^2)\right]\left[1 + \cos 2\frac{\pi yx}{\lambda} \cdot V\right] \quad , \qquad (10)$$

and

$$I_{s_2} = I_{o_2} K_{o_2} d^2 \exp\left[\left(-\frac{2}{b_{o_2}^2}\right)(x^2+y^2)\right] \quad , \qquad (11)$$

where

$$Ko = \frac{1}{4r^2}\int_{A_{lens}} \left\{ \left[\varepsilon^2(\theta,n)\, D(\theta)\right]_{refraction} + \left[\varepsilon^2(\theta,n)\, D(\theta)\right]_{reflection} + \left[\frac{J_1^2(\alpha\sin\theta)}{\sin^2\theta}\right]_{diff.} \right\} dA \quad . \qquad (12)$$

K_o is a scattering coefficient, D is the divergence, n the index of refraction, ε the fraction of energy for every ray reflected or refracted, d is the diameter of a spherical particle, V is its

visibility, r the distance from the scattering center to the collecting lens, and θ the collection angle measured from the forward direction. It can be shown[15] that the contributions of these three terms is a function of angle. To keep the following analysis simple we will choose a collection angle θ of 30°. Assuming that the solid angle of the collecting lens is small with respect to θ we can then compare the intensities scattered at the discrete angle θ.

The refraction or reflection terms are given by:

$$i_R = a^2 \varepsilon^2 D \quad ,$$

and the diffraction by:

$$i_D = \frac{\alpha^2}{\sin^2\theta} J_1^2 (\alpha \sin\theta) \quad .$$

where $\alpha = \frac{\pi d}{\lambda}$ is the size parameter, and J_1 the Bessel's function of the first kind. Reference 9 shows that for S polarization:

$$i(\text{refraction}) = 1.0375\ \alpha^2$$
$$i(\text{reflection}) = 0.0785\ \alpha^2$$

and it can be calculated that

$i_D(\alpha) < .088\ \alpha^{-2}$ for $\alpha > 49$ ($d > 7.6\ \mu m$). At this angle the combined reflected and diffracted light represent 16% of the refracted light. Which implies that in general the three components must be taken into account. It is assumed that the collecting lens is in the plane of symmetry of the crossing beams. The above equations show that the scattered light intensity is proportional to the square of the diameter of the sphere. This approximation is only valid for diameters larger than about 10 wavelengths. Note that the angle θ (deviation of incident pencil of light) to an arbitrary position of the lens is different for both beams (except on the line of symmetry). However, the integrated value is the same as long as the collecting lens is in the plane of symmetry. In this technique the ac modulation of I_{s_1} is used to establish detectability of the signal and to measure the velocity. For a given threshold level, the larger the dynamic size range, the farther from the center of the beam the largest particle can cross and still exhibit ac modulation and, therefore, be detectable. This will introduce an error in the measurement as will be discussed in the next section.

The peak to peak ac signal is then given by:

$$I_{ac_1} = 4\, I_{o_1} K_{o_1} Vd^2 \exp\left[\left(-\frac{2}{b_{o_1}^2}\right)(x^2+y^2)\right] \quad . \tag{13}$$

and the pedestal is given by:

$$P_1 = 2I_{o_1} K_{o_1} d^2 \exp\left[\left(-\frac{2}{b_{o_1}^2}\right)(x^2 + y^2)\right] \quad . \tag{14}$$

Dynamic size range and error analysis

There are two known sources of error in the IMAX method. First is the error introduced by beam blockage produced by other particles in the trajectory of the beams and scattered light. This one is difficult to quantify and will be discussed with the results. Second, since the small beam has a finite diameter the particles can travel a small distance away from the center of the big beam and still cross sufficient fringes to be detectable. The farther from the center it can be detectable, the larger the error it can produce. It will be shown here that this error increases with dynamic size range, and decreases with ratio of the large to small beam.

The dynamic range is limited by the electronic and optical noise. In general, we can establish that there is a threshold to the minimum processible ac signal, and a saturation level associated with the largest signal processible by the electronics. All the processible signals must fall between these two limits. Equation 13 gives the peak to peak ac signal. Notice that both the diameter (d) and the visibility (V) influence the above expression.

To simplify this analysis we will neglect the contribution of diffraction, that is the collection angle will be off-axis. Single particle counters usually collect off-axis light ($\theta > 30°$) for the sake

of producing a small probe volume. Therefore, the above assumption is very reasonable for spheres larger than 7 μm. The dynamic range is actually larger when diffraction is included.

The minimum processible ac signal is produced by the smallest particle (with diameter d_{min}) crossing the probe volume at y = o and crossing the minimum number of fringes required by the electronics ($x = b_{o_1}$).

Therefore, $I_{ac_{min}} = 4I_{o_1}K_{o_1}d_{min}^2 \exp(-2)$ where it has been assumed that the visibility of the smallest particle is 1.

The maximum ac signal is produced by a droplet of diameter d_o (not necessarily d_{max}) and visibility V_o.

$$I_{ac_{max}} = 4I_{o_1}K_{o_1}d_o^2V_o \exp\left[\left(-\frac{2}{b_{o_1}^2}\right)\left(x^2+y^2\right)\right] \quad . \tag{15}$$

The farthest from the center this particle can be detected is when:

$$I_{ac_{max}} = I_{ac_{min}}$$

and it crosses sufficient number of fringe ($x = b_{o_1}$). Therefore,

$$4I_{o_1}K_{o_1}d_o^2 \exp\left[\left(-\frac{2}{b_{o_1}^2}\right)\left(b_{o_1}^2+y^2\right)\right] = 4I_{o_1}K_{o_1}d_{min}^2 \exp(-2) \quad .$$

Solving for the size range, we obtain:

$$\left(\frac{d_o}{d_{min}}\right) = \frac{\exp(-2)}{V_o} \exp\left[\frac{2\left(b_{o_1}^2 + y^2\right)}{b_{o_1}^2}\right] = \frac{1}{V_o} \exp\left(\frac{2y^2}{b_{o_1}^2}\right) \quad ,$$

and

$$2y^2 = b_{o_1}^2 \, \ell n\left[\left(\frac{d_o}{d_{min}}\right)^2 \frac{V_o}{\exp(-2)}\right] - 2\, b_{o_1}^2 \quad ,$$

which results in

$$2y^2 = b_{o_1}^2 \, \ell n\left[V_o\left(\frac{d_o}{d_{min}}\right)^2\right] \quad . \tag{16}$$

The error in the size will be due to an error in the intensity scattered by the large beam when the particle crosses at $y > o$ (notice that the particle must cross through $x = 0$). If we state that the large beam is m times larger than the small one,

$$\frac{I_{s_2}}{I_{o_2} K_{o_2} d^2} = \exp\left(\frac{-2y^2}{m^2 b_{o_1}^2}\right) \quad . \tag{17}$$

To simplify the error analysis, let us assume that the optical parameters are chosen such that for any size range the visibility of the largest droplet is larger than zero.

That is $V(d_{max}) > 0$ and $d'_{max} < 1$ where $d'_{max} = 1$ produces the first zero in the visibility. Then the maximum ac signal is produced by a particle of diameter $d_o = 0.626\ d_{max}$ and its visibility is 43%.

Substituting these values into Equation 16, we obtain:

$$\frac{2y^2}{b_{o_1}^2} = \ln\left[.1685\left(\frac{d_{max}}{d_{min}}\right)^2\right] \quad .$$

The maximum errors resulting from the finite size of the beams can now be presented in tabular form.

m	d_{max}/d_{min}	$\frac{2y^2}{b_{o_1}^2}$	$\frac{I_{s_2}}{I_{o_2} K_{o_2}^2}$	max error
7	10	2.82	.94	3%
7	20	4.21	.92	4%
7	30	5.02	.90	5%
5	10	2.82	.89	5%
5	20	4.21	.85	8%
5	30	5.02	.82	10%

5.2 Single Color System

Figure 5.2 shows a schematic representation of the probe volume formed by crossing two beams of the same wavelength but different

diameters. There are several fundamental differences between this and the two color system: 1) Fringes are formed everywhere the large and small beams mix; 2) The pedestal of the large beams can not be spectrally separated but electronically filtered. The intensity distibution of either beam can be expressed as:

$$I_1 = I_{o_1} \exp\left[-\frac{2}{b_{o_1}^2}\left(x^2+y^2\right)\right] \quad , \tag{18}$$

and

$$I_2 = I_{o_2} \exp\left[-\frac{2}{b_{o_2}^2}\left(x^2+y^2\right)\right] \quad . \tag{19}$$

The intensity scattered by the spherical particle can be expressed by:

$$I_s = I_{s_1} + I_{s_2} + 2\sqrt{I_{s_1} I_{s_2}}\cos\beta \cdot V$$

where

$$I_s = IK_o d^2 \quad .$$

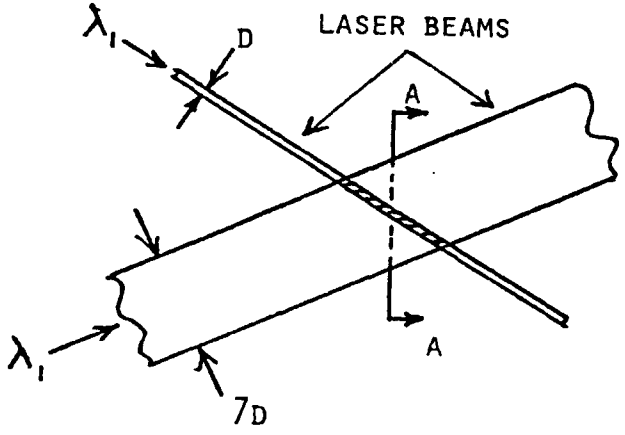

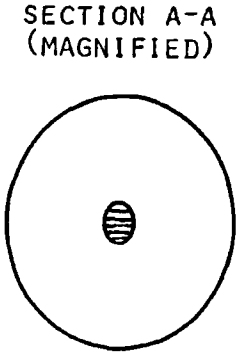

FIGURE 5.2. PROBE VOLUME OF SINGLE COLOR IMAX TECHNIQUE.

CFH-19

β is the phase angle, and again it is assumed that the collecting lens is on the plane of symmetry of the two crossing beams. The pedestal is given by

$$P = I_{s_1} + I_{s_2}$$

and the peak to peak ac intensity:

$$I_{ac} = 2\sqrt{I_{s_1} I_{s_2}}\, V\,(\cos\beta = 1) - 2\sqrt{I_{s_1} I_{s_2}}\, V\,(\cos\beta = -1)$$

$$= 4\sqrt{I_{s_1} I_{s_2}}\, V \quad .$$

That is,

$$P = I_{o_1} K_o d^2 \exp\left[-\frac{2}{b_{o_1}^2}(x^2+y^2)\right] + I_{o_2} K_o d^2 \exp\left[-\frac{2}{b_{o_2}^2}(x^2+y^2)\right] \quad , \qquad (20)$$

and

$$I_{ac} = 4K_o\sqrt{I_{o_1} I_{o_2}}\, d^2 V \exp\left[-\frac{(x^2+y^2)}{b_{o_1}^2} - \frac{(x^2+y^2)}{b_{o_2}^2}\right] \quad . \qquad (21)$$

Following the same approach as before, and again neglecting the contribution of diffraction for the off-axis collection angle. If we let $m = b_{o_2}/b_{o_1}$, we obtain:

$$I_{ac_{min}} = 4K_o\sqrt{I_{o_2} I_{o_2}}\, d_{min}^2 \exp\left[-1 - \frac{1}{m^2}\right] \quad , \tag{22}$$

$$I_{ac_{max}} = 4K_o\sqrt{I_{o_1} I_{o_2}}\, d_o^2 V_o \exp\left[-\frac{\left(b_{o_1}^2 + y^2\right)}{b_{o_1}^2} - \frac{\left(b_{o_1}^2 + y^2\right)}{m^2 b_{o_1}^2}\right] \quad . \tag{23}$$

The variation in y will result in an error of the measured pedestal. If we can assume that m is large, then the pedestal of the large beam can be recovered by electronic filtering and it is given by the second term of Equation 20. This variation in y is obtained equating 22 and 23, and we obtain

$$y^2 = \frac{m^2 b_{o_1}^2}{m^2+1} \ln\left[\frac{d_o^2 V_o}{d_{min}^2}\right] \quad . \tag{24}$$

The error in the size will result from droplets crossing the pedestal of the large beam at x = o and y given by 24. That is:

$$\frac{I_{s_2}}{I_{o_2} K_o d^2} = \left[\frac{-2y^2}{m^2 b_{o_1}^2}\right] \quad . \tag{25}$$

Making similar assumptions as before:

$$d_o = .626\, d_{max} \text{ and } V_o = 0.43$$

$$\therefore \frac{2y^2}{m^2 b_{o_1}^2} = \frac{2}{m^2+1} \ln \left[.1685 \left(\frac{d_{max}}{d_{min}} \right)^2 \right] \quad . \qquad (26)$$

The maximum errors resulting from the finite size of the beams can be presented in tabular form:

m	d_{max}/d_{min}	$\frac{2y^2}{m^2 b_{o_1}^2}$	$\frac{I_{s_2}}{I_{o_2} K_{o_2} d^2}$	max error
7	10	.113	.89	5%
7	20	.168	.84	8%
7	30	.2	.82	10%
5	10	.22	.80	10%
5	20	.32	.72	15%
5	30	.39	.68	18%

It should be pointed out that the technique discussed here bases the detectability of the signal on the modulated or ac part of the scattered light. It is, therefore, important that no zeros are present in the visibility function.

5.3 A Self-Calibrating Algorithm Combining IMAX with V/I

SPC's based on absolute scattered light require calibration at one datum point. When measuring dense sprays beam attenuation will make this calibration difficult. An algorithm is discused here that will eliminate this problem.

The algorithm is based on measuring the visibility of any size class droplet. Combining the visibility and intensity[16] of the signal a very accurate measurement of such size can be made. Knowing the size of the chosen corresponding visibility one can then establish the amplitude of the pedestal of this signal by adjusting the gain to the photo detector. The logic is as follows: for a given visibility (chosen in the most accurate region of the visibility function) there is an associated size and, therefore, an intensity scattered from the large beam. Since the intensity of this large beam is almost uniform the scattered light associated with the chosen visibility will be almost constant in the absence of errors in the visibility. There are, however, errors associated with measuring visibility in a dense spray and these points are rejected by V/I[16]. The process is an iterative one where V/I is implemented by choosing several narrow intensity bands to establish points out of control. The gain to the photo-detector is adjusted until the majority of the points fall in the pre-established intensity band corresponding to the measured size.

5.4 The IMAX Probe Volume

The dynamic range exercise indicated that droplets that scatter light with large modulation are detectable over a larger region than

those that scatter light with little modulation. As a result, the probe volume or region of detectability is a function of droplet size. Algorithms have been presented[17] to define the probe volume in LDV type systems. A very simple algorithm will be presented here for the two color system and off-axis collection.

Notice that only the small beams define the probe volume in this case and, therefore, the probe volume will be a standard LDV type volume. The approach followed will be very similar to the one described in Reference (17).

There are two signal levels imposed by the electronics: the saturation (I_{max}) and the threshold (I_{min}). The intensity to the peak of the ac modulation (I_{peak}) of the largest signal must be less than I_{max}, and the smallest detectable signal must be larger than I_{min} (defined peak to peak).

$$I_{peak_1} = 2I_{o_1} K_{o_1} d_o^2 \left(1+V_o\right) < I_{max} \quad . \tag{27}$$

where d_o produces the largest signal within the detectable size range, and V_o is its corresponding visibility.

Solving for I_{o_1} we obtain:

$$I_{o_1} = \frac{I_{max}}{2K_{o_1} d_o^2 \left(1+V_o\right)} \quad . \tag{28}$$

This expression can now be substituted in Equation 13 to obtain:

$$I_{ac_1} = \frac{2d^2 \, V \, I_{max}}{d_o^2 \, (1+V_o)} \exp \left[\left(- \frac{2}{b_{o_1}^2} \right) (x^2+y^2) \right] \quad , \tag{29}$$

and the detectability criterion establishes that $I_{ac_1} > I_{min}$ and that sufficient fringes are crossed. If we assume that the number of fringes processed by the electronics is equal to that in the waist diameter, $x = b_{o_1}$.

Solving for y in Equation 29 we obtain:

$$y < \sqrt{- \frac{b_{o_1}^2}{2} \ln \left[\frac{I_{min}}{2I_{max}} \left(\frac{d_o}{d} \right)^2 \frac{(1+V_o)}{V} \right] - b_{o_1}^2} \quad . \tag{30}$$

The cross-sectional area of sensitivity for an off-axis pinhole limited signal can be approximated by:

$$A(d) = \frac{2D_p y}{\sin\theta} \cdot \frac{f_1}{f_2} \quad , \tag{31}$$

where D_p is the pinhole diameter and f_1/f_2 determines the magnification of the receiving optics. The effect of the pinhole and the coordinate system are illustrated on Figure 5.3.

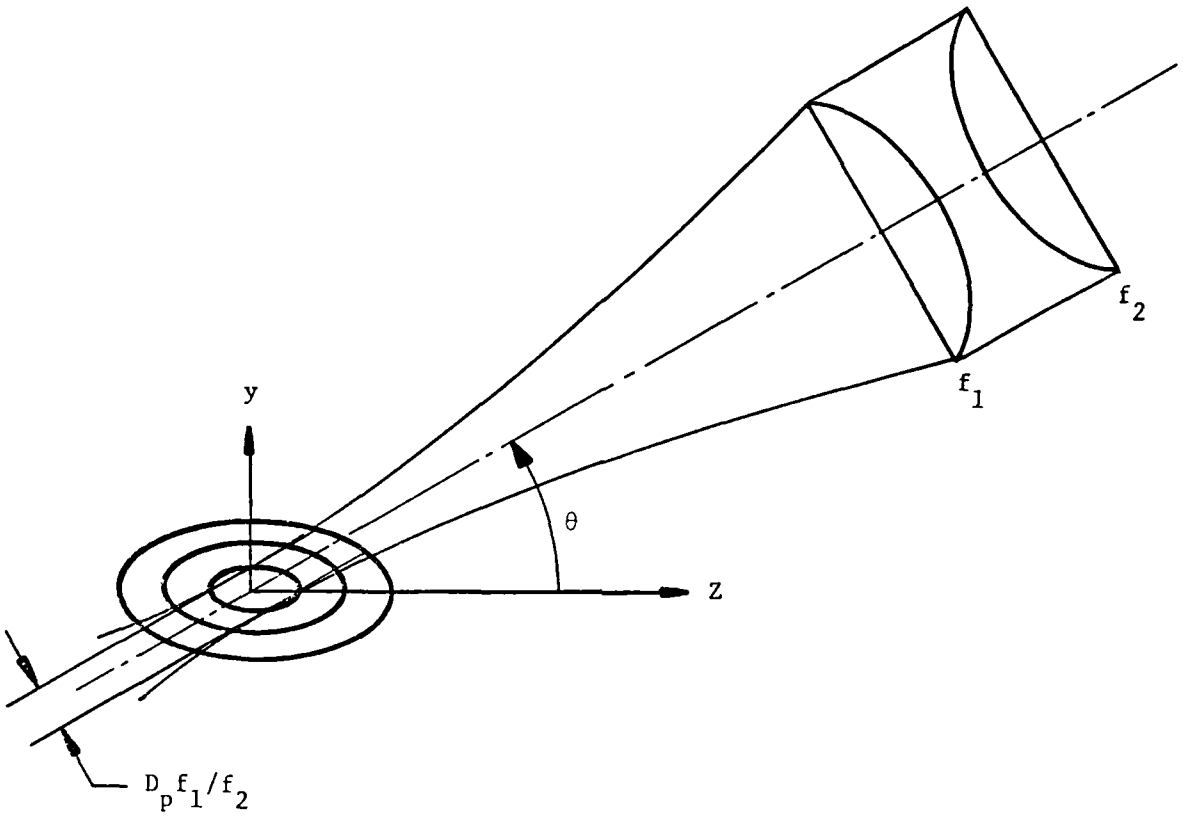

FIGURE 5.3. SCHEMATIC REPRESENTATION OF DUAL BEAM PROBE VOLUME LIMITED BY A PINHOLE.

As seen by Equation 30 and 31 the area of detectability (in the y,z plane) is only a function of droplet size and corresponding visibility. This area can now be normalized and provide a weighting function to size distributions otherwise biased to the large signals.

This weighting factor is given by:

$$w(d) = \frac{A(d)}{A_{max}} \quad .$$

The number density of any size droplet can also be calculated by dividing the number of counts of the given size by its corresponding sampling volume (SV).

The sampling volume is a cylinder with cross-section A(d) and length equal to the droplet velocity (U(d)) multiplied by the effective sampling time (T).

That is $SV(d) = A(d)U(d)T$, and $T = TS - \sum_{i=1}^{M} N\,\tau D_i - M\tau_o$, where TS is the total sampling time to collect M samples, N is the number of fringes, τD_i is the Doppler period of sample i and τ_o is the processor's dead time after every sample.

The number density of size d is then given by:

$$ND(d) = \frac{N(d)}{A_{max}U(d)T} \quad , \qquad (32)$$

where n(d) is the raw count of size d. Because of the multivalued characteristic of the visibility curve, V_o should be larger than the first zero of the visibility function. Equation (10) defines the abscissa of this function as $d' = \frac{d}{\delta CF}$. This value should be kept smaller than one, however physical constraints render this not always possible. The collection factor (CF) can be easily changed almost linearly by changing the collection F#. In the experiments reported here this was done by placing a mask on the path of light scattered by the small beams. As an example, the spray data shown on Figures 5.9A and 5.9B correspond to $I_{min} = .6 \times 10^{-3}$ V, $I_{max} = .7$ V (these intensities are read directly in volts). Since very little data was measured above 160 μm, the mask was chosen to obtain d' = 1 at about 160 μm. Therefore $d_o' = \frac{200}{\delta CF} = \frac{200}{160} = 1.24$. The following values are then obtained for the nondimensional diameter (d'), its visibility (V) and the normal probe volume dimension (y, as given by Equation 30).

d	20	40	60	80	100	120	140	160	180	200
d'	.12	.25	.37	.5	.62	.75	.87	1.0	1.12	1.24
V	.97	.88	.76	.6	.43	.27	.12	.02	.08	.12
y	.35	.9	1.06	1.14	1.17	1.15	1.03	.55	1.05	1.19

Similar calculations were performed for the size ranges 5 to 50 μm, and 10 to 100 μm.

5.5 Description of IMAX Breadboard

Figure 5.4 shows a schematic diagram of the two-color breadboard system. An argon-ion laser provides the light source. The beam colors are separated by the dispersion prism and two of these colors (the 5145Å shown by the broken line, and the 4880Å shown by the solid line) are used to define the probe volume. A beam expander formed by lenses L1 and L2 define the beam ratio parameter m. A compensated beamsplitter splits the blue beam into two beams and the transmitting lens L3 focuses and crosses these two blue beams in the middle of the green beam. The receiving optics use a dichroic mirror to separate the two colors of the scattered light. The probe volume is imaged on pinholes in front of two PMT's and interference filters are used to perfectly separate the two colors. The outputs of the two PMT's are then electronically processed as shown on Figure 5.5, and information of the size and velocity of individual spheres crossing the probe volume is thus obtained. An electronic processor was developed for this purpose, and a dedicated microprocessor was interfaced to store, display and analyze the acquired data. Sample rates of several KHz are possible with this system.

5.6 Results Obtained with the IMAX Technique.

Experimental results are presented to illustrate the accuracy and resolution of the IMAX technique.

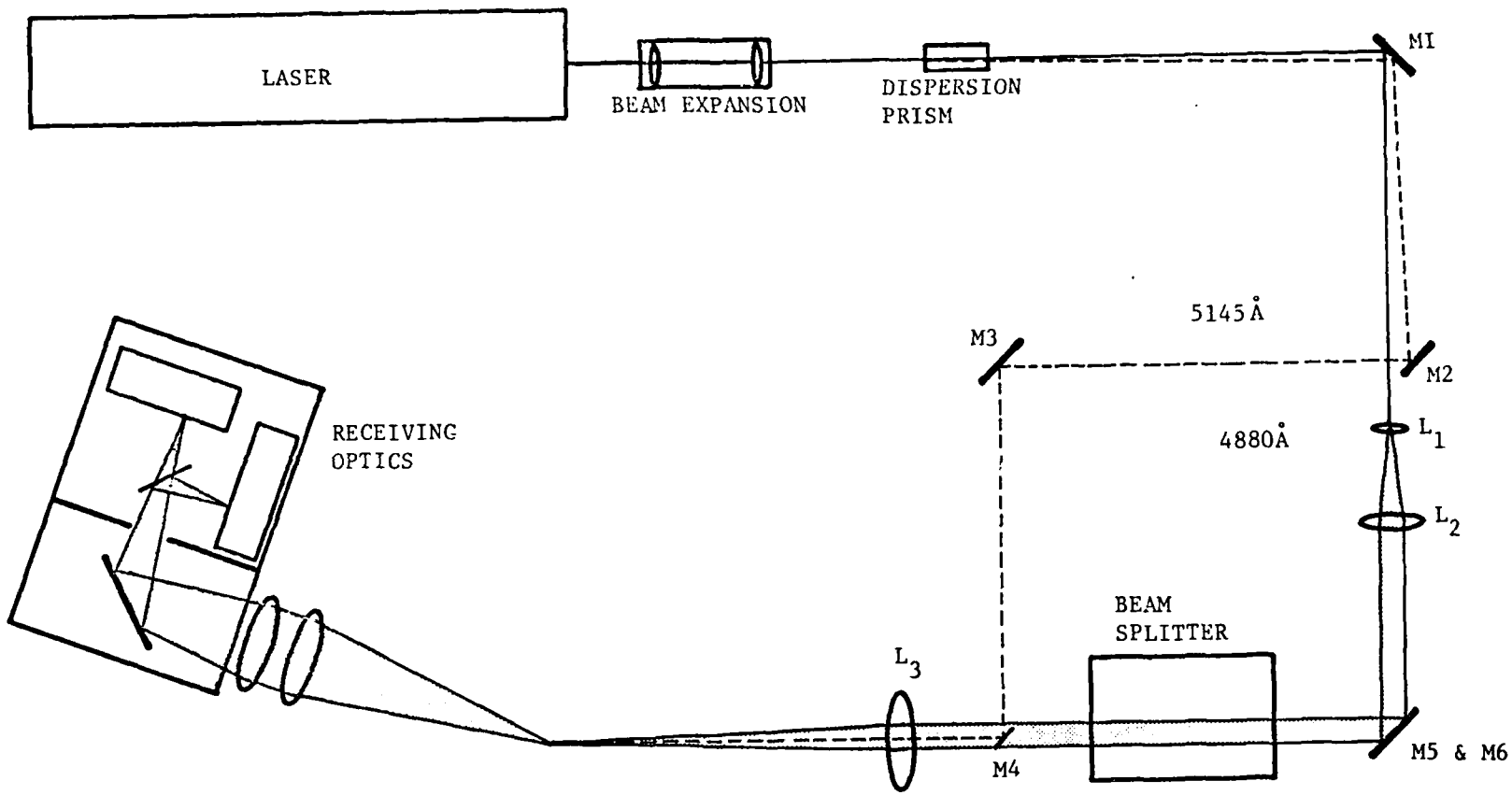

FIGURE 5.4. SCHEMATIC IMAX BREADBOARD SYSTEM

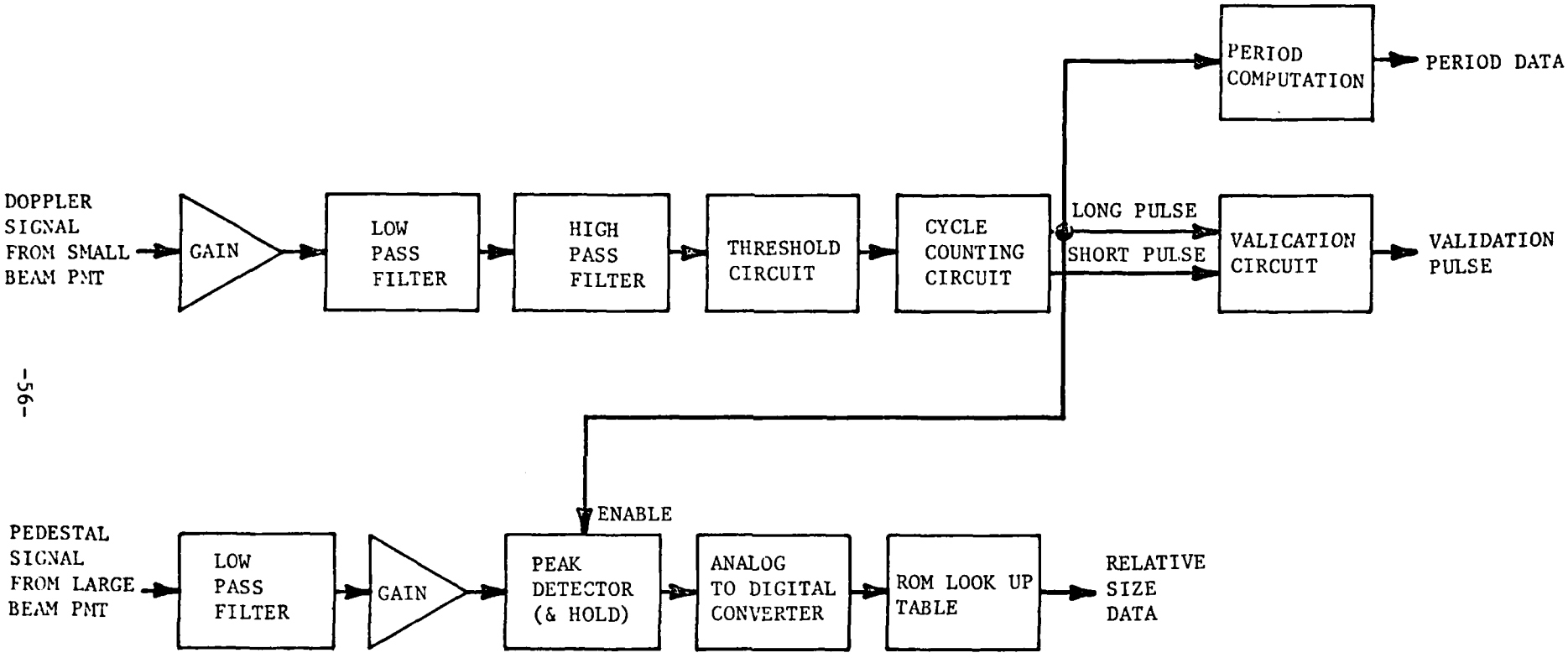

FIGURE 5.5. ELECTRONICS BLOCK DIAGRAM
DROPLET SIZING, TWO COLOR IMAX TECHNIQUE

IMAX Measurements with the Berglund Liu Droplet Generator

A vibrating orifice droplet generator was used to produce strings and sprays of known size droplets. The procedure used in these experiments was to produce a string of large monodispersed droplets to calibrate the instrument. Smaller droplets were then produced by increasing the frequency of vibration of the orifice, and with the dispersion air a spray of these droplets was formed. The spray angle was about 10° and the number density was typically 500/cm^3. The optical configuration consisted of a transmitting lens of 711 mm, m = 7, blue waist diameter of 100 μm, receiving angle of 20°, and receiving lenses of 300/495 mm. The calibration point was provided by a string of 110 μm droplets produced with a flow rate of 0.21 cm^3/min and a frequency of 5 KHz. Figure 5.6 shows the measured size and velocity. A spray of primary droplets of 49 μm (produced with a flow rate of 0.21 cm^3/min and frequency of 56.9 KHz) was then produced with the dispersion air. Figure 5.7a shows the measurements of the spray of primary droplets. Figure 5.7b shows the measurements of a spray formed of primary droplets and doublets. The theoretically predicted sizes are 49 μm and 62 μm. The sizes actually measured were 46 μm and 57 μm respectively. Figure 5.7c extends the measurements of 7b to the presence of triplets. The theoretically predicted sizes in this case are 49 μm, 62 μm and 70 μm. Note that the measured diameters of the doublets and triplets are related to the primary droplets by $2^{1/3}$ and $3^{1/3}$ respectively.

FIGURE 5.6. IMAX MEASUREMENTS ON STRING OF MONODISPERSED DROPLETS

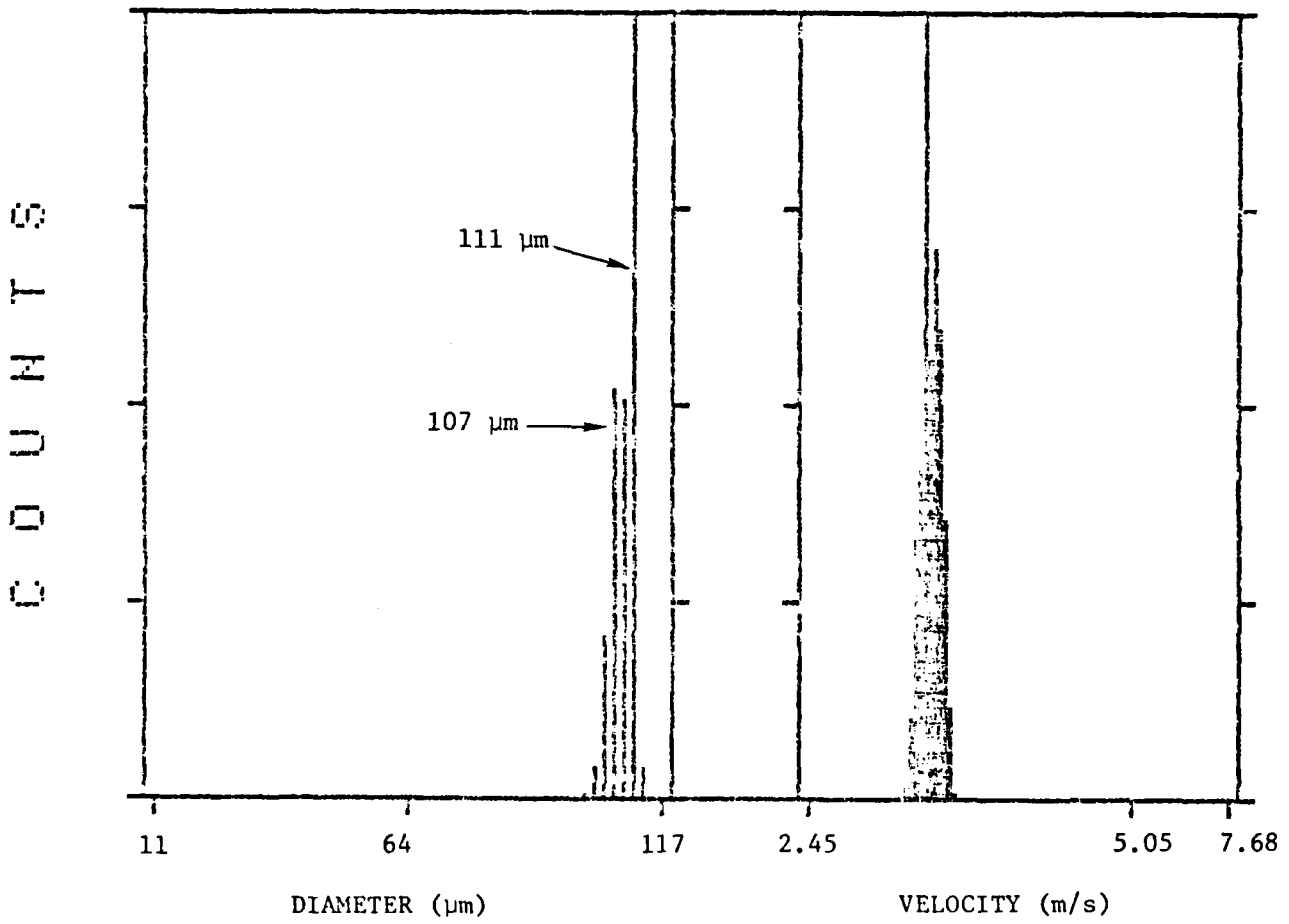

IMAX DROPLET SIZE MEASUREMENTS

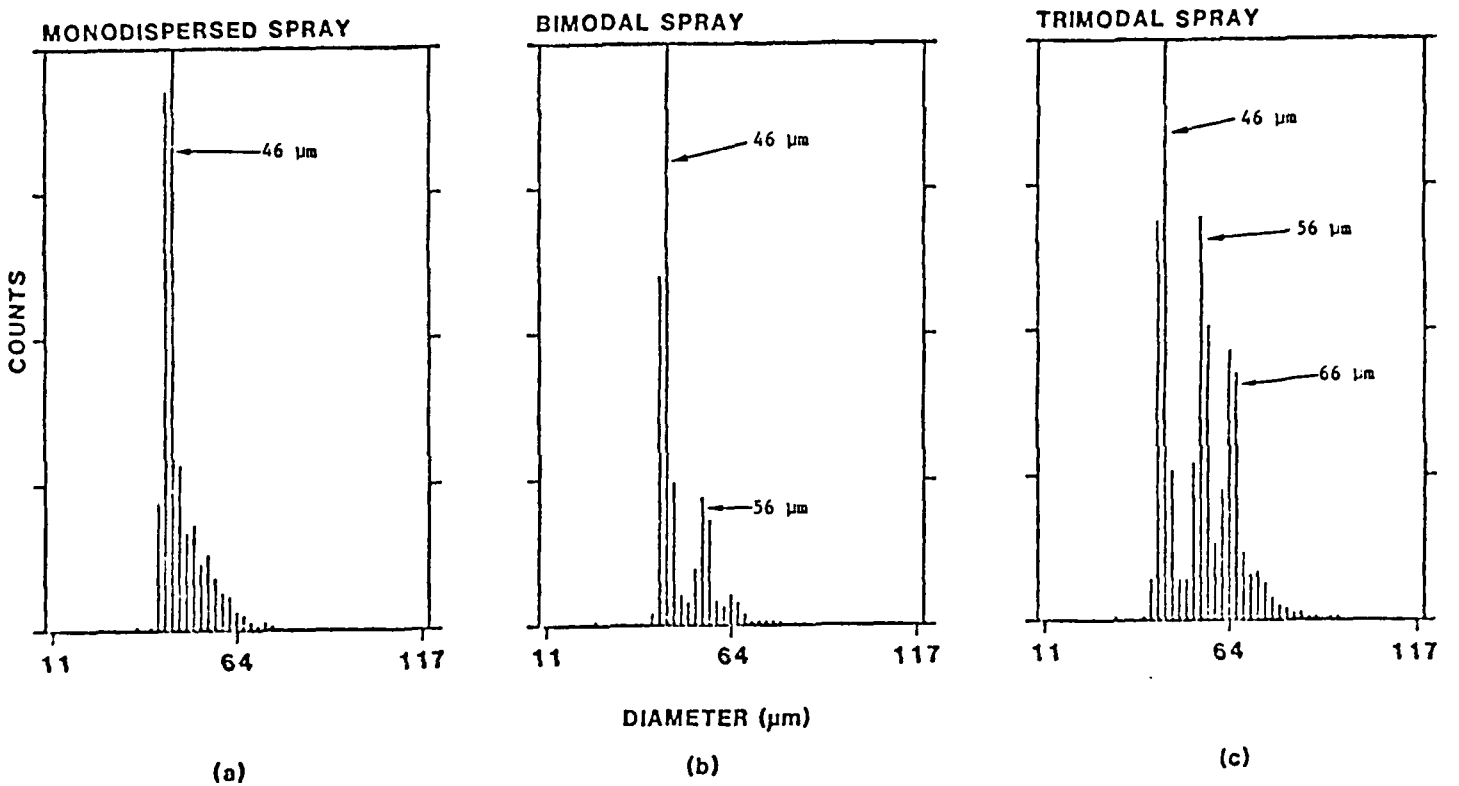

83-2263-15M (OS)

FIGURE 5.7.

Effect of beam blockage on size distribution

The effect of spray blocking the laser beams before they cross on the size distribution measured with IMAX was explored. A size range of 10 to 100 μm was used in this case, and the monodispersed droplet size was 73 μm.

Figure 5.8a shows the measurement of the monodispersed string of droplets.

Figure 5.8b shows similar results but a spray is blocking the laser beams. Two effects can be noted: the peak of the distribution dropped to 69 μm (5%) and the spread of the distribution is +5 μm, -7 μm (+7%, -10%), to the $1/e^2$. It should be noted that once the high voltage is corrected to account for the beam blockage, the broadening should have very little effect in the distribution of a polydispersed spray.

Spray measurements with IMAX

Measurements of a spray produced by a pressure nozzle (Spraying Systems TG0.3 at 50 psi) were conducted with IMAX. They were made at 30 mm from the nozzle tip and at two radii: 0 and 10 mm. The results are shown on Figures 5.9a and 5.9b. The trend shown by the two plots is the expected one. That is, there are more small droplets in the middle of the spray than on the edge.

In order to test the resolution of the system, data were obtained using three different size ranges: 5 to 50 μm; 10 to 100 μm; and 20 to 200 μm. This is one of the most difficult self-consistency tests imposed on any technique, and most available techniques will show a

EFFECT OF BEAM BLOCKAGE ON SIZE DISTRIBUTION

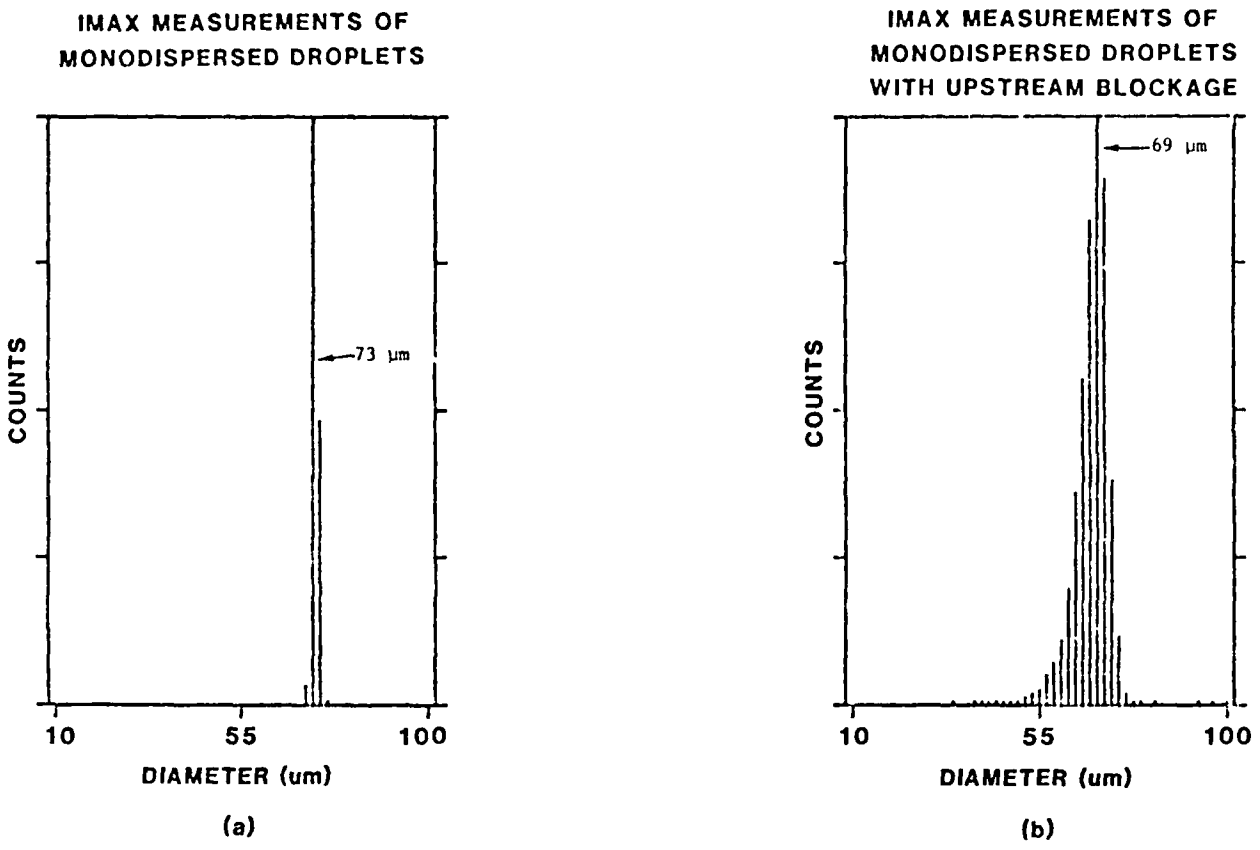

FIGURE 5.8

SPRAY CHARACTERIZATION WITH IMAX

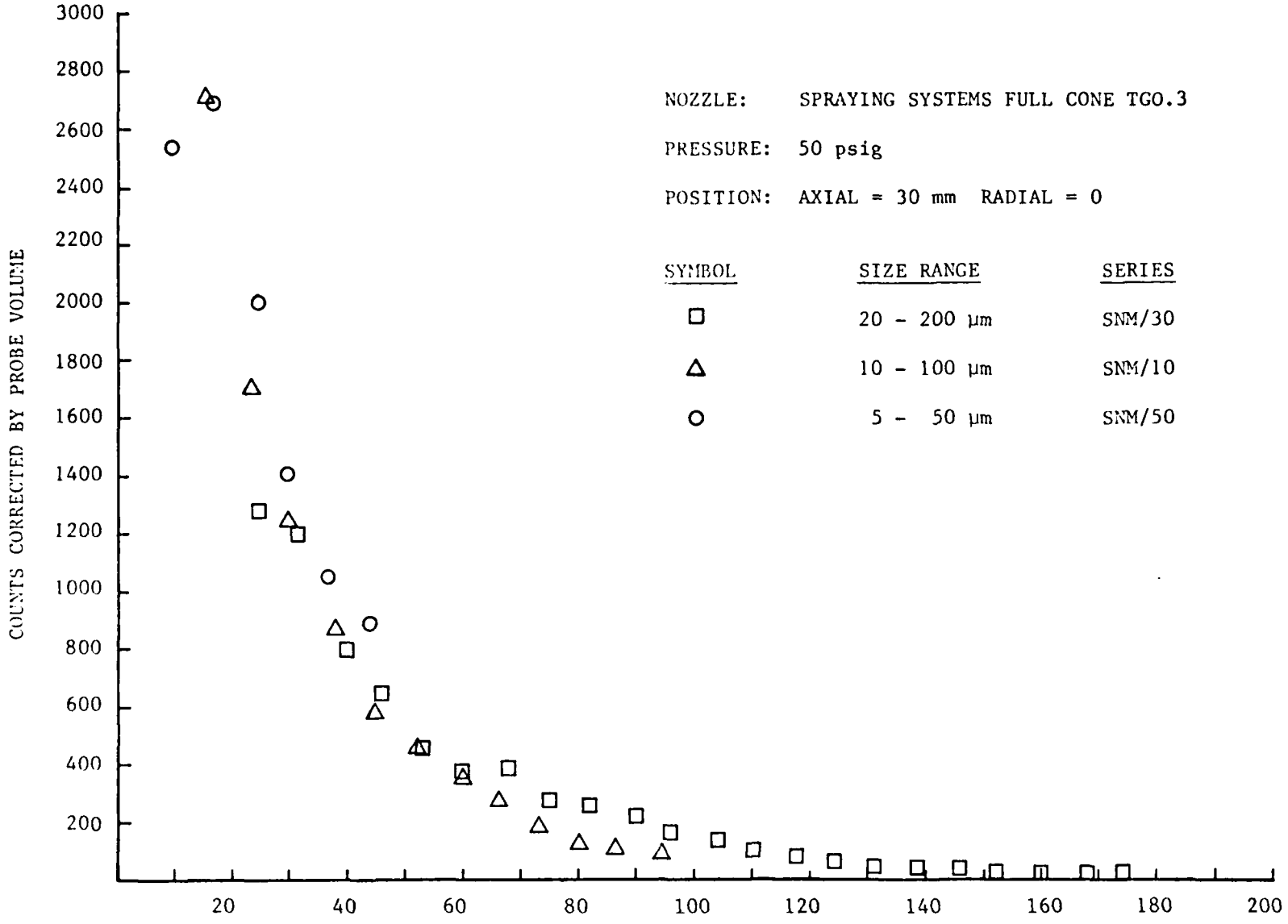

Figure 5.9a

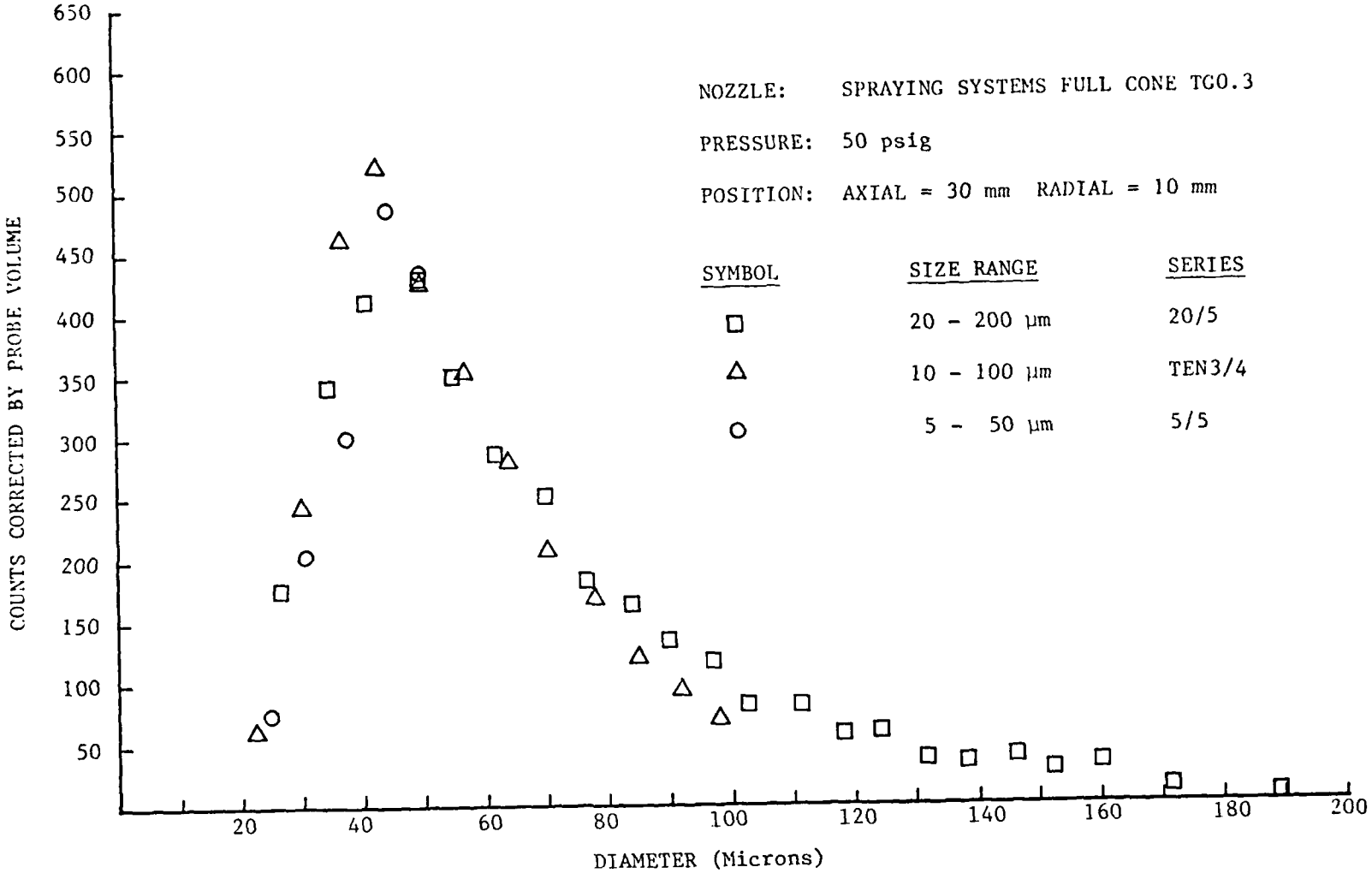
NOZZLE: SPRAYING SYSTEMS FULL CONE TG0.3
PRESSURE: 50 psig
POSITION: AXIAL = 30 mm RADIAL = 10 mm
SYMBOL
SIZE RANGE
SERIES
20 - 200 µm
20/5
10 - 100 µm
TEN3/4
5 - 50 µm
5/5
COUNTS CORRECTED BY PROBE VOLUME
650
600
550
500
450
400
350
300
250
200
150
100
50
20
40
60
80
100
120
140
160
180
200
DIAMETER (Microns)

Figure 5.9b

shift on the predicted data. IMAX shows excellent matching of the data in the overlapping region as illustrated in Figures 5.9a and 5.9b.

The corresponding droplet velocity distributions are shown on Figures 5.10a and 5.10b. It can be observed that the droplets are moving faster at the edge of the spray than in the center. This results from the large momentum and terminal velocity associated with the large droplets present at the edge of the spray.

SPRAY VELOCITY DISTRIBUTION WITH IMAX

NOZZLE: SPRAYING SYSTEMS FULL CONE TGO.3

PRESSURE: 50 psig

AXIAL POSITION: 30 mm

RADIAL POSITION: 0

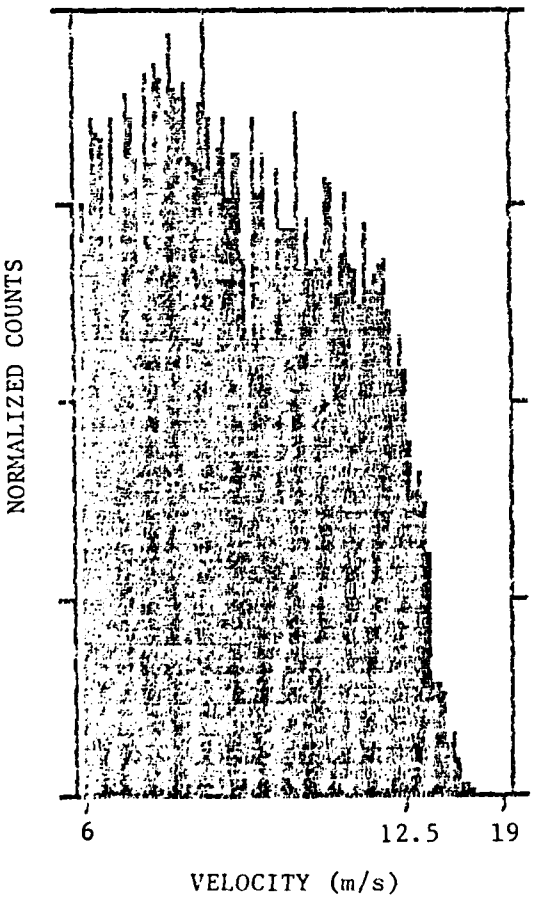

Figure 5.10a

RADIAL POSITION: 10 mm

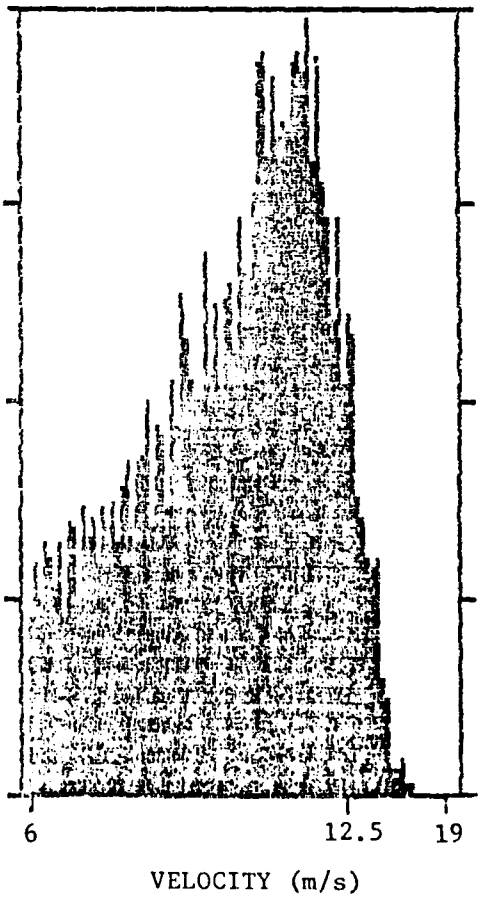

Figure 5.10b

6.0 PUBLICATIONS

1. C. F. Hess, "A Technique Combining the Visibility of a Doppler Signal with the Peak Intensity of the Pedestal to Measure the Size and Velocity of Droplets in a Spray", AIAA Paper Number 84-0203, presented at AIAA 22nd Aerospace Sciences Meeting, January 9-12, 1984/Reno, Nevada.

Publications in Progress

1. C. F. Hess, "A Nonintrusive Optical Single Particle Counter for Measuring the Size and Velocity of Droplets in a Spray", submitted to Applied Optics (1984)

2. C. F. Hess and V. Espinosa, "Spray Measurements with a Nonintrusive Optical Scattering Technique". Submitted to Optical Engineering.

7.0 PROFESSIONAL PERSONNEL

Cecil F. Hess, Ph.D.	Principal Investigator
Victor Espinosa	Research Assistant

REFERENCES

1. W. M. Farmer, Applied Optics, Vol. 11, No. 11, (1972).

2. D. M. Robinson and W. P. Chu, Applied Optics, Vol. 14, 2177 (1975).

3. R. T. Adrian and K. L. Orloff, Applied Optics, Vol. 16, No. 3 (1977).

4. D. W. Roberds, "Particle Sizing Using Laser Interferometry", Applied Optics, Vol. 16, No. 7 (1976).

5. W. D. Bachalo, Applied Optics, Vol. 19, No. 3 (1980).

6. J. D. Pendleton, Applied Optics, Vol. 21, No. 4. (1982).

7. M. L. Yeoman, B. J. Azzopardi, H. J. White, C. J. Bates and P. J. Roberts, "Eng. Appl. of Laser Velocimetry" Winter Annual Meeting ASME. Phoenix, Arizona, November 14-19 (1982).

8. B. H. Liu, R. N. Berglund, J. K. Argawal, Atmospheric Environment, Vol. 8, pp. 717-732 (1974).

9. A. J. Yule, N. A. Chigier, S. Atakan, and A. Ungut, J. Energy 1, 220-228 (1977).

10. D. Holve and S. A. Self, Appl. Opt. 18 (1979).

11. Y. Mizutani, H. Kodama and K. Miyasaka, Combustion and Flame 44:85-95 (1982).

12. A. Men', Y. Krimerman, and D. Adler, J. Phys. E.:Sci. Instrum. 14 (1981).

13. P. R. Ereaut, A. Ungut, A. J. Yule, N. Chigier, Proceedings from "The 2nd International Conference of Liquid Atomization and Spray Systems", p. 261 (1982).

14. W. J. Glantschnig, M. W. Golay, S. H. Chen, and F. R. Best, Appl. Opt. 21 (1982).

15. H. C. van de Hulst, "Light Scattering by Small Particles" John Wiley and Sons, 1957, Chap. 12.

16. C. F. Hess, AIAA 22nd Aerospace Sciences Meeting, AIAA-84-0203 (1984).

17. D. W. Roberts, C. W. Brasier, and B. W. Bomar, Opt. Eng. 18 (1979).